

3D Stress Analysis of Adhesively Bonded Composite Joints

Jian Zhang[‡]

Collier Research Corp., Hampton, VA 23669

Brett A. Bednarczyk[§]

University of Virginia, Charlottesville, VA 22903

Craig Collier^{**} and Phil Yarrington^{††}

Craig.collier@hypersizer.com

Collier Research Corp., Hampton, VA 23669

Yogesh Bansal^{‡‡} and Marek-Jerzy Pindera^{§§}

University of Virginia, Charlottesville, VA 22903

A robust and rapid analytical method for 3D stress analysis of composite bonded joints has been recently developed based on Mortensen's unified approach, with considerable extension to accommodate hygrothermal loads and most importantly, to compute the in-plane and out-of-plane, through-the-thickness interlaminar peel and shear stresses in the laminate adherends. Compared to other analytical methods for bonded joint analysis the present method is capable of handling more general situations, including various joint geometries, both linear and nonlinear adhesive, asymmetric and unbalanced laminates, and more general loading and boundary conditions. The formulation has been extended from strict cylindrical bending to consider generalized cylindrical bending that allows an arbitrary constant strain to be applied in the out-of-plane direction. Other analytical methods, such as Hart-Smith's, are 1-D and mainly focus on obtaining adhesive stresses, while generally ignoring stresses in laminate adherends, particularly interlaminar stresses, which are known to be key contributors to failure. Joining composite structures using adhesive bonding remains a challenging problem because performance is severely influenced by the characteristics of the composite laminate adherends, which usually have low interlaminar strengths. This new method, most importantly, computes local 3D stress fields in each ply of each adherend, which vary along the joint. Given the realistic 3D local stress fields at the ply level within each adherend, failure criteria can be employed to predict joint strength, which can facilitate better joint designs. This paper addresses the computation of stresses for composite bonded doubler joints. A companion paper, also presented in this conference, addresses failure prediction.

I. Introduction

Adhesively composite joints have been widely used in modern lightweight flight and space vehicle structures and will be more heavily used in the next generation of aircraft, on vehicles such as the Joint Strike Fighter (JSF), Long Range Strike (LRS) aircraft, and new Unmanned Aerial Vehicles (UAV). However, designing composite bonded joints is challenging because their performance is limited by the characteristics of the composite laminate adherends, which usually have low interlaminar strengths. The interlaminar stresses induced in the vicinity of the bondline

Copyright 2005 by Collier Research Corporation. Published by the AIAA, Inc., with permission

[‡] Research Engineer, 2 Eaton St., Suite 504, Hampton, VA 23669, AIAA Member.

[§] OAI Senior Research Scientist, Department of Civil Engineering, AIAA Member.

^{**} Senior Research Engineer, 2 Eaton St., Suite 504, Hampton, VA 23669, AIAA Senior Member.

^{††} Senior Research Engineer, 2 Eaton St., Suite 504, Hampton, VA 23669, AIAA Member.

^{‡‡} Research Assistant, Applied Mechanics, Thornton Hall B228, 351 McCormick Road, Charlottesville, VA 22904

^{§§} Professor, Department of Civil Engineering.

leading edges of joints can then cause delamination of the laminated adherends. Thus, accurate 3D stress analysis is essential for understanding the failure of bonded composite joints. While tools exist for rapid design, analysis, and sizing of aerospace structures from the vehicle global level to the local stiffened panel component (e.g. HyperSizer®, Collier Research Corp.), a weak link in the design process remains the automated sizing of joints between structural components and between stiffened panel facesheets and stiffeners. Hence, methods that address this gap are needed to enable rapid estimates of joint stress fields, strengths, and margins of safety.

The adhesively bonded joint problem is typically approached in one of two ways; with finite element analysis or through analytical modeling. Finite element analysis has the advantage of geometric flexibility and the availability of commercial finite element codes. Examples of finite element investigations of adhesively bonded composite joints include Kairouz and Matthews², Sheno and Hawkins³, Tsai et al.⁴, Yamazaki and Tsubosaka⁵, Tong⁶, Li, et al.⁷, Krueger et al.^{9,10}, Bogdanovich and Kizhakkethara¹¹, and others. The literature shows that standard h-based finite element codes can accurately predict the local stress fields within adhesively bonded joints under arbitrary loading conditions. P-based finite element codes such as StressCheck¹² improve local field predictions by altering the order of the elements' polynomials rather than requiring successively finer element meshes to capture concentrations. As such, the Composites Affordability Initiative (CAI) has selected StressCheck as a potential design tool for adhesively bonded joints. The drawbacks to using FEA for bonded joint design are in efficiency and mesh dependence. In design and sizing, many different joint configurations must be analyzed quickly, and each finite element model can take hours or even days to properly pre- and post-process. Second, because the stress gradients for bonded joints can be very steep, especially at the reentrant corner, the accuracy of the method can be highly dependent on mesh refinement.

Analytical approaches to bonded joint analysis employ simplifying assumptions in terms of the joint geometry, loading, and resultant local fields in order to formulate efficient closed-form elasticity solutions for the local fields in the joint region. The advantage of analytically modeling the bonded joints is that each joint configuration can be analyzed in a matter of seconds or even fractions of a second. These approaches have roots in classical shear-lag analysis of Volkersen¹³ and the work of Goland and Reissner¹⁴, who accounted for bending in the analysis of a bonded single lap joint. Hart-Smith¹⁵⁻²⁰ extended these solutions to account for the inelastic behavior of the adhesive and considered many different joint configurations. However, these formulations have traditionally been limited by the types applied loading considered and by the 1-D treatment of the adherends with an effective stiffness in the joint direction. Delale et al.²¹ developed a close-form solution for lap-shear joints with orthotropic adherends using classical plate theory. Oplinger²² developed a layered beam analysis, which included treatment of large deflections. The above analytical methods mainly focus on obtaining the adhesive stresses, while generally ignoring stresses in the adherends, particularly the interlaminar stresses, which are known to be the key contributors to failure of laminated adherends.

More recently, Mortensen²³ and Mortensen and Thomsen^{24,25} presented a unified analytical approach to analyze an array of common bonded joint configurations for more general loading conditions. Mortensen's treatment also considers arbitrary laminate adherends (based on classical lamination theory) and solves for the distributions of the normal and shear force and moment resultants along the joint in both adherends as well as peel and shear stress distributions in the adhesive. Further, through the application of an efficient solution algorithm, convergence issues that sometimes arise in Hart-Smith's formulation have been overcome. However, the full stress fields, in particular the interlaminar stresses, throughout the adherends are still not resolved through Mortensen's approach.

This paper presents a new capability for the design and analysis of bonded joints based on extensions to the Mortensen's unified approach. This new method has been incorporated within the HyperSizer® structural sizing software framework. The basic features of the Mortensen's approach have been retained. A wide range of joint types may be considered, and the adherends can be unbalanced and/or unsymmetric laminates. Both linear and nonlinear behavior of the adhesive layer is admitted in the analysis. For linear analysis, the adhesive layer is modeled as continuously distributed linear tension/compression and shear springs. Inclusion of nonlinear adhesive behavior in the analysis is accomplished through the use of a secant modulus approach for the nonlinear tensile stress-strain relationship in conjunction with a yield criterion. Finally, the equilibrium equations for each joint are derived, and by combination of these equations and relations, a set of governing ordinary differential equations is obtained. The governing system of equations is solved numerically using the 'multi-segment method of integration,'²³ yielding laminate-level fields and adhesive stresses that vary both through the thickness and along the joint in each adherend.

Several extensions to the original approach have greatly enhanced HyperSizer's usefulness for sizing and design of adhesive joints in real aerospace applications. First, the formulation has been extended from strict cylindrical bending to consider generalized cylindrical bending that allows an arbitrary constant strain to be applied in the out-of-plane direction. Second, hygrothermal effects have been incorporated within the method. Third, and most

importantly, HyperSizer computes the local 3D stress fields in each ply of each adherend, including both in-plane stresses and out-of-plane interlaminar stresses. Computation of these stresses allows the implementation of failure criteria for predicting bond strength, thus enabling joint design.

The present investigation employs HyperSizer to analyze composite bonded doubler joints. Results of in-plane and out-of-plane stresses within the adherends, together with adhesive stresses, are plotted and compared to both h-based and p-based finite element results, both of which considered elastic adhesive behavior. Results of this paper indicate that HyperSizer is an efficient and accurate tool for the 3D stress analysis of adhesively bonded joints.

II. Description of HyperSizer Method

A. Basic assumptions for the structural modeling of bonded joints

The basic restrictive assumptions of HyperSizer for the structural modeling of bonded joints are summarized as the follows. Note, the coordinate system for the bonded joint analysis is shown in Figure 1.

The adherends:

- Plates in generalized cylindrical bending, which allows for uniform strain applied in the transverse direction.
- Generally orthotropic laminates using Classical Lamination Theory (CLT).
- Strains and rotations are assumed to be small.

The adhesive layer:

- Modeled as continuously distributed linear tension/compression and shear springs.
- Inclusion of non-linear adhesive behavior via a non-linear secant modulus approach.

Loading and boundary conditions:

- General boundary and loading conditions. One of each pair in the following can be applied at the joint boundaries: (1) longitudinal (x) midplane displacement or axial unit force (u_0 or N_x); (2) in-plane transverse displacement or shear force (v_0 or N_{xy}); (3) vertical deflection or transverse shear unit force (w or Q_x); (4) longitudinal curvature or bending moment (β_x or M_x)
- Hygrothermal load: uniform temperature change ΔT and/or uniform moisture content Δc change.
- In the transverse (y) direction, uniform strain e_0 can be applied.
- Reaction forces and moments, M_y, M_{xy}, N_y are calculated.

HyperSizer's analysis method has been implemented for eight types of bonded joints: single-lap and double-lap joints with straight or scarfed adherends, bonded doubler with straight or stepped adherends, single and double-sided scarfed lap joints.

B. Adherends as plates in generalized cylindrical bending

Modified from Mortensen's²³ original cylindrical bending assumptions for the adherends, the generalized cylindrical bending conditions treat the adherends and joint as a wide plate, where the longitudinal (x -direction) displacement and vertical deflection can be described as a function of the x coordinate only, while the in-plane transverse (y -direction) displacement can accommodate generalized plane strains in addition to the longitudinal field (see Fig. 1). As a consequence, longitudinal displacements will be uniform along the y direction, while the in-plane transverse displacement varies linearly along the width (y) direction. This displacement field can be described as:

$$u_0^i = u_0^i(x) \quad v_0^i = e_0^i y + v_0^i(x) \quad w^i = w^i(x) \quad (1)$$

where u_0 is the mid-plane displacement in the x direction, v_0 is the midplane displacement in the y direction, w is the displacement in the out-of plane transverse direction (z), and e_0 is the uniform strain in the y direction. The displacement components in each laminate, u_0, v_0, w , are all defined relative to the middle surface of each laminate, and i corresponds to the laminate/adherend number.

Considering that the adherends are subjected to both mechanical and non-mechanical loads (i.e., hygrothermal strains), the constitutive equations for the laminated adherends are given as:

$$N_{xx}^i = A_{11}^i u_{0,x}^i + A_{12}^i e_0^i + A_{16}^i v_{0,x}^i - B_{11}^i w_{,xx}^i - N_{xx}^{i*}$$

$$\begin{aligned}
N_{yy}^i &= A_{12}^i u_{0,x}^i + A_{22}^i e_0^i + A_{26}^i v_{0,x}^i - B_{12}^i w_{,xx}^i - N_{yy}^{i*} \\
N_{xy}^i &= A_{16}^i u_{0,x}^i + A_{26}^i e_0^i + A_{66}^i v_{0,x}^i - B_{16}^i w_{,xx}^i - N_{xy}^{i*} \\
M_{xx}^i &= B_{11}^i u_{0,x}^i + B_{12}^i e_0^i + B_{16}^i v_{0,x}^i - D_{11}^i w_{,xx}^i - M_{xx}^{i*} \\
M_{yy}^i &= B_{12}^i u_{0,x}^i + B_{22}^i e_0^i + B_{26}^i v_{0,x}^i - D_{12}^i w_{,xx}^i - M_{yy}^{i*} \\
M_{xy}^i &= B_{16}^i u_{0,x}^i + B_{26}^i e_0^i + B_{66}^i v_{0,x}^i - D_{16}^i w_{,xx}^i - M_{xy}^{i*}
\end{aligned} \tag{2}$$

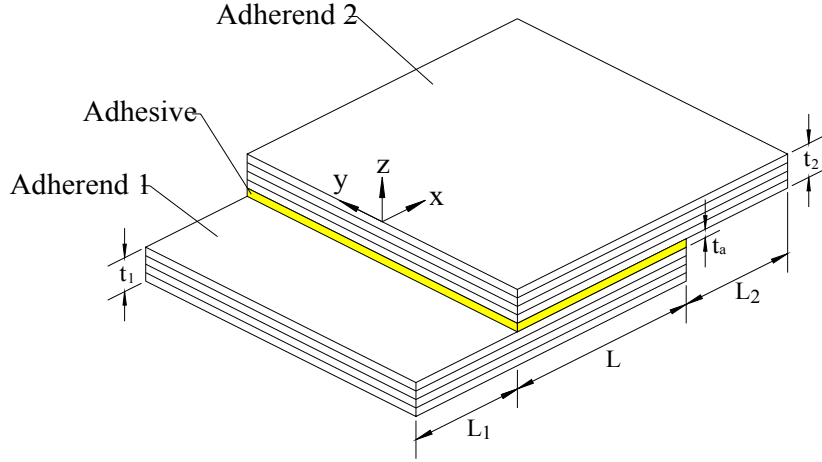


Fig. 1 Schematic illustration of an adhesive single lap joint with straight adherends in the overlap zone.

where i represents the adherend number and A_{jk}^i , B_{jk}^i and D_{jk}^i ($j, k = 1, 2, 6$) are the extensional, coupling and flexural rigidities. N_{xx}^i , N_{yy}^i , N_{xy}^i , M_{xx}^i , M_{yy}^i , and M_{xy}^i are the in-plane force and moment resultants, and N_{xx}^{i*} , N_{yy}^{i*} , N_{xy}^{i*} , M_{xx}^{i*} , M_{yy}^{i*} , and M_{xy}^{i*} are the in-plane hygrothermal force and moment resultants. Note that ‘ x ’ and ‘ $,xx$ ’ subscripts in Eq.(2) indicate first and second derivatives with respect to x , respectively. Employing CLT, the hygrothermal terms are given as

$$N_n^* = \sum_{k=1}^N \{ \bar{Q}_{nm}^{(k)} \cdot \varepsilon_m^{(k)*} \cdot t_k \} \quad \text{and} \quad M_n^* = \sum_{k=1}^N \{ \bar{Q}_{nm}^{(k)} \cdot \varepsilon_m^{(k)*} \cdot (z_k^2 - z_{k-1}^2) / 2 \} \tag{3}$$

where $\varepsilon_m^{(k)*}$ is the in-plane hygrothermal strain vector in each ply, i.e., $\varepsilon_m^{(k)*} = \alpha_m^{(k)} \Delta T + \beta_m^{(k)} \Delta c$. $\alpha_m^{(k)}$ and $\beta_m^{(k)}$ are the coefficients of thermal and moisture expansion, and ΔT and Δc are the changes in temperature and moisture content.

For advanced joint types such as a scarfed or stepped lap, the rigidities A_{jk}^i , B_{jk}^i and D_{jk}^i ($j, k = 1, 2, 6$) are determined as functions of the x direction of the joint within the overlap zone, since the adherend thicknesses are allowed to vary within the overlap. From the Kirchhoff-Love assumptions, the following kinematics relations for the laminates are derived:

$$u^i = u_0^i + z \beta_x^i, \quad \beta_x^i = -w_{,x}^i, \quad \beta_y^i = 0 \tag{4}$$

where u^i is the x displacement at any z location, u_0^i is the longitudinal displacement at the adherend mid-plane, and w_i is the vertical displacement of the i^{th} adherend. β_x^i and β_y^i are the slopes in the two directions.

C. Constitutive relations for the adhesive layer

Linear spring adhesive model

The coupling between the adherends is established through the constitutive relations for the adhesive layer, which, as a first approximation, is assumed to be homogeneous, isotropic and linear elastic. The constitutive relations for the adhesive layer are established by use of a two-parameter elastic foundation approach, where the adhesive layer is assumed to be composed of continuously distributed shear and tension/compression springs. The constitutive relations of the adhesive layer are given as

$$\begin{aligned}\tau_{ax} &= G_a \cdot \gamma_{ax} = \frac{G_a}{t_a} (u^i - u^j) \\ \tau_{ay} &= G_a \cdot \gamma_{ay} = \frac{G_a}{t_a} (v^i - v^j) \\ \sigma_a &= E_a \cdot \varepsilon_{az} = \frac{E_a}{t_a} (w^i - w^j)\end{aligned}\tag{5}$$

where i and j are the adherend numbers, τ_{ax} , τ_{ay} , σ_a , γ_{ax} , γ_{ay} , and ε_{az} are the adhesive shear and normal stresses and strains, and G_a and E_a are the shear and elastic modulus of the adhesive layer.

Non-linear adhesive model

Most polymeric structural adhesives exhibit inelastic behavior in the sense that local permanent plastic strains are induced even at low levels of external loading. Thus, nonlinear adhesive behavior must be considered if a more realistic response of bonded joints is sought. The nonlinear adhesive behavior can be modeled with a measured true stress-strain curve, either in pure tension or in pure shear, and a mathematical model that takes the multi-axial stress state into account. The measured stress-strain curves can be characterized by a variety of mathematical models for the sake of analytical and numerical analysis. In HyperSizer, several commonly used mathematical models are employed to characterize this nonlinear behavior, including elastic-perfectly plastic, bilinear, and Ramberg-Osgood. The solution procedure for non-linear adhesives is described fully in Collier's complete report on this method.²⁶

D. Equilibrium equations

The equilibrium equations are derived based on equilibrium elements inside and outside the overlap zone for each of the considered joint types. The equilibrium equations are derived for plates in generalized cylindrical bending. The general equilibrium equations outside the overlap zone for each of the adherends (Fig. 1),

$$\begin{aligned}N_{xx,x}^i &= 0 \\ N_{xy,x}^i &= 0 \\ Q_{x,x}^i &= 0 && \text{outside the overlap zone} \\ M_{xx,x}^i &= Q_x^i \\ M_{xy,x}^i &= Q_y^i\end{aligned}\tag{6}$$

where i corresponds to the adherends, in general, $i=1, 2, 3$.

In generalized cylindrical bending the force and moment resultants are only a function of x , and their derivatives with respect to y are all equal to zero. The equilibrium equations derived inside the overlap zones can be divided into the following two groups:

- Joints with one adhesive layer inside the overlap zone.
- Joints with two adhesive layers inside the overlap zone.

These two groups are further divided into joints with straight or scarfed adherends within the overlap. However, in the following only the equilibrium equations for joints with two straight adherends within the overlap will be shown, i.e. single lap joint (see Fig. 1), bonded doubler and single sided stepped lap joint. For a full description of the derivation of the equilibrium equations for other joint types, see Mortensen²³.

$$\begin{aligned}
N_{xx,x}^1 &= -\tau_{ax}, & N_{xx,x}^2 &= \tau_{ax}, \\
N_{xy,x}^1 &= -\tau_{ay}, & N_{xy,x}^2 &= \tau_{ay}, \\
Q_{x,x}^1 &= -\sigma_a, & Q_{x,x}^2 &= \sigma_a, \\
M_{xx,x}^1 &= Q_x^1 - \tau_{ax} \cdot \frac{t_1(x) + t_a}{2}, & M_{xx,x}^2 &= Q_x^2 - \tau_{ax} \cdot \frac{t_2(x) + t_a}{2}, \\
M_{xy,x}^1 &= Q_y^1 - \tau_{ay} \cdot \frac{t_1(x) + t_a}{2}, & M_{xy,x}^2 &= Q_y^2 - \tau_{ay} \cdot \frac{t_2(x) + t_a}{2}
\end{aligned} \tag{7}$$

where $t_1(x)$ and $t_2(x)$ are the adherend thicknesses and t_a is the adhesive layer thickness. For single lap joints and bonded doubler joints the adherend thicknesses constant throughout the overlap zone; for stepped lap joints, the adherend thicknesses may change inside the overlap zone between each step.

From the equations given above, it is possible to form a complete system of governing equations for each of the bonded joint configurations. That is, combination of the constitutive and kinematics relations, together with the constitutive relations for the adhesive layers, and the equilibrium equations lead to a set of 8 coupled linear first-order ordinary differential equations describing the system behavior of each adherend. The system equations are solved numerically using Mortensen's multi-segment method. For details on the system of governing equations and the multi-segment solution method, see Mortensen²³.

E. In-plane stresses in the adherends

The adherend lay-up sign convention and associated coordinate system is shown in Fig. 2. The in-plane stresses and strains in the laminated adherends are obtained directly from CLT, in which the Kirchhoff-Love linear assumption is applied, i.e., $\gamma_{yz} = \gamma_{zx} = 0$ and $\varepsilon_z = 0$. This assumption leads to the linear relation between the displacement field of the laminate and the mid-plane displacement,

$$\begin{aligned}
w(x, y, z) &= w^0 \\
u(x, y, z) &= u^0 - z \frac{\partial w}{\partial x} \\
v(x, y, z) &= v^0 - z \frac{\partial w}{\partial y}
\end{aligned} \tag{8}$$

The in-plane strain fields in each laminate can thus be derived from the standard kinematics relations. They are

$$\begin{aligned}
\varepsilon_x &= \frac{\partial u}{\partial x} = \frac{\partial u^0}{\partial x} + z \left(-\frac{\partial^2 w}{\partial x^2} \right) = \varepsilon_x^0 + z \kappa_x \\
\varepsilon_y &= \frac{\partial v}{\partial y} = \frac{\partial v^0}{\partial y} + z \left(-\frac{\partial^2 w}{\partial y^2} \right) = \varepsilon_y^0 + z \kappa_y \\
\gamma_{xy} &= \frac{\partial v}{\partial x} + \frac{\partial u}{\partial y} = \frac{\partial v^0}{\partial x} + \frac{\partial u^0}{\partial y} + z \left(-2 \frac{\partial^2 w}{\partial x \partial y} \right) = \gamma_{xy}^0 + z \kappa_{xy}
\end{aligned} \tag{9}$$

where $\boldsymbol{\varepsilon}^0 = \{\varepsilon_x^0, \varepsilon_y^0, \varepsilon_z^0\}$ is the strain of the mid-plane and $\boldsymbol{\kappa} = \{\kappa_x, \kappa_y, \kappa_{xy}\}$ is the curvature of the mid-plane. The in-plane strain of an arbitrary point in the laminate can be obtained through Eq.(9) once the mid-plane strain is known. The latter can be determined from the overall equilibrium and constitutive equation of the laminate.

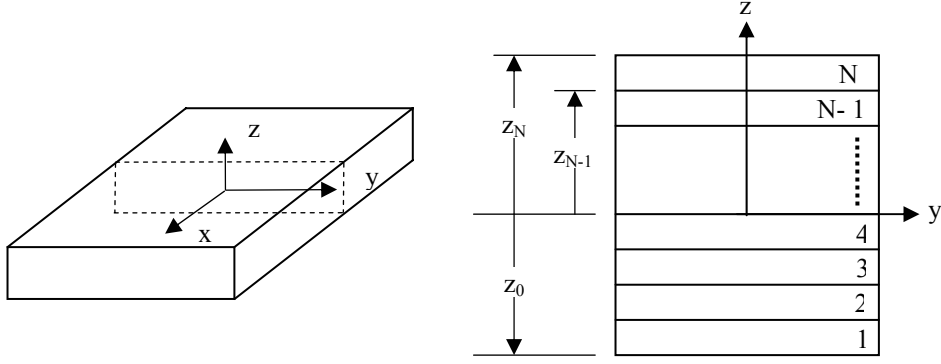


Fig. 2 Lay-up of a laminate and the coordinate system.

Under the assumption of generalized cylindrical bending, the mid-plane displacements are given in the forms as following

$$u^0 = u^0(x) \quad v^0 = e_0 y + v^0(x) \quad w^0 = w^0(x) \quad (10)$$

Thus, Eq. (9) can be reduced to

$$\begin{aligned} \varepsilon_{xx} &= \frac{\partial u^0}{\partial x} + z \left(-\frac{\partial^2 w}{\partial x^2} \right) = u_{,x}^0 + z \beta_{x,x} \\ \varepsilon_{yy} &= \frac{\partial v^0}{\partial y} + z \left(-\frac{\partial^2 w}{\partial y^2} \right) = e_0 \\ \gamma_{xy} &= \frac{\partial v^0}{\partial x} + \frac{\partial u^0}{\partial y} + z \left(-2 \frac{\partial^2 w}{\partial x \partial y} \right) = v_{,x}^0 \end{aligned} \quad (11)$$

The in-plane stress components of the laminated adherends can be obtained through the constitutive equation for each ply. Including the hygrothermal effect, the in-plane stresses of the k th ply are given by

$$\begin{bmatrix} \sigma_{xx} \\ \sigma_{yy} \\ \tau_{xy} \end{bmatrix}^{(k)} = \begin{bmatrix} \bar{Q}_{11} & \bar{Q}_{12} & \bar{Q}_{16} \\ \bar{Q}_{21} & \bar{Q}_{22} & \bar{Q}_{26} \\ \bar{Q}_{61} & \bar{Q}_{62} & \bar{Q}_{66} \end{bmatrix}^{(k)} \left\{ \begin{bmatrix} \varepsilon_{xx} \\ \varepsilon_{yy} \\ \gamma_{xy} \end{bmatrix} - \begin{bmatrix} \varepsilon_{xx}^* \\ \varepsilon_{yy}^* \\ \gamma_{xy}^* \end{bmatrix} \right\}^{(k)} \quad (12)$$

where ε_{ij}^* is the hygrothermal strain, which is given by

$$\begin{bmatrix} \varepsilon_{xx}^* \\ \varepsilon_{yy}^* \\ \gamma_{xy}^* \end{bmatrix} = \Delta T \begin{bmatrix} \alpha_x \\ \alpha_y \\ \alpha_s \end{bmatrix} + \Delta c \begin{bmatrix} \zeta_x \\ \zeta_y \\ \zeta_s \end{bmatrix} \quad (13)$$

where α_j and ζ_j are the coefficients of thermal and moisture expansion, respectively.

F. Out-of-plane (Interlaminar) stresses in the adherends

Even though CLT does not account for the out-of-plane response, the out-of-plane stresses can be calculated approximately using the local equilibrium equations. Without body force, the standard equilibrium equations are written as

$$\begin{aligned}\frac{\partial \sigma_{xx}}{\partial x} + \frac{\partial \tau_{xy}}{\partial y} + \frac{\partial \tau_{xz}}{\partial z} &= 0 \\ \frac{\partial \tau_{xy}}{\partial x} + \frac{\partial \sigma_{yy}}{\partial y} + \frac{\partial \tau_{yz}}{\partial z} &= 0 \\ \frac{\partial \sigma_{zz}}{\partial z} + \frac{\partial \tau_{yz}}{\partial y} + \frac{\partial \tau_{xz}}{\partial x} &= 0\end{aligned}\quad (14)$$

Under the assumptions of generalized cylindrical bending, $\frac{\partial \sigma_{yy}}{\partial y} = \frac{\partial \tau_{yz}}{\partial y} = \frac{\partial \tau_{xy}}{\partial y} = 0$. Thus, the out-of-plane stress components can be obtained via integration of the simplified equilibrium equations Eq.(14),

$$\begin{aligned}\tau_{xz} &= - \int_{free\ surface}^{\bar{z}} \left(\frac{\partial \sigma_{xx}}{\partial x} \right) dz \\ \tau_{yz} &= - \int_{free\ surface}^{\bar{z}} \left(\frac{\partial \tau_{xy}}{\partial x} \right) dz \\ \sigma_{zz} &= - \int_{free\ surface}^{\bar{z}} \left(\frac{\partial \tau_{xz}}{\partial x} \right) dz\end{aligned}\quad (15)$$

by requiring these stress components to vanish at the adherend free surfaces. One simple way to calculate the out-of-plane stresses is to integrate Eq.(15) numerically. However, in the present formulation, large oscillations result due to lack of continuity of the x -derivatives of $\{u^0, v^0, w^0, \beta_x, N_{xx}, N_{xy}, M_{xx}, Q_x\}$ computed by using Mortensen's multi-segment integration method²³. In order to overcome this oscillation problem, some algebra is required to avoid using the discontinuous numerical derivatives from the multi-segment solutions. First, Eq.(12) is expanded and the in-plane stress components σ_{xx} and τ_{xy} are written as

$$\begin{aligned}\sigma_{xx}^{(k)} &= \bar{Q}_{11}^{(k)} [\varepsilon_{xx}^{(k)} - \varepsilon_{xx}^{(k)*}] + \bar{Q}_{12}^{(k)} [\varepsilon_{yy}^{(k)} - \varepsilon_{yy}^{(k)*}] + \bar{Q}_{16}^{(k)} [\gamma_{xy}^{(k)} - \gamma_{xy}^{(k)*}] \\ &= \bar{Q}_{11}^{(k)} \{ (u_{,x}^0 + z^{(k)} \beta_{x,xx}) - \varepsilon_{xx}^{(k)*} \} + \bar{Q}_{12}^{(k)} [e_0 - \varepsilon_{yy}^{(k)*}] + \bar{Q}_{16}^{(k)} [v_{,x}^0 - \gamma_{xy}^{(k)*}]\end{aligned}\quad (16)$$

$$\begin{aligned}\tau_{xy}^{(k)} &= \bar{Q}_{16}^{(k)} [\varepsilon_{xx}^{(k)} - \varepsilon_{xx}^{(k)*}] + \bar{Q}_{26}^{(k)} [\varepsilon_{yy}^{(k)} - \varepsilon_{yy}^{(k)*}] + \bar{Q}_{66}^{(k)} [\gamma_{xy}^{(k)} - \gamma_{xy}^{(k)*}] \\ &= \bar{Q}_{16}^{(k)} \{ (u_{,x}^0 + z^{(k)} \beta_{x,xx}) - \varepsilon_{xx}^{(k)*} \} + \bar{Q}_{26}^{(k)} [e_0 - \varepsilon_{yy}^{(k)*}] + \bar{Q}_{66}^{(k)} [v_{,x}^0 - \gamma_{xy}^{(k)*}]\end{aligned}\quad (17)$$

Assuming the hygrothermal strains are constant in each ply, the derivatives of σ_{xx} and τ_{xy} and the integrals appearing in Eq. (15) are then given as

$$\frac{\partial \sigma_{xx}^{(k)}}{\partial x} = \bar{Q}_{11}^{(k)} [u_{,xx}^0 + z^{(k)} \beta_{x,xxx}] + \bar{Q}_{16}^{(k)} [v_{,xx}^0] \quad (18-1)$$

$$\int_{free}^{\bar{z}} \frac{\partial \sigma_{xx}^{(k)}}{\partial x} dz = \sum_{k=1}^i \bar{Q}_{11}^{(k)} [(z^{(k+1)} - z^{(k)}) u_{,xx}^0 + \frac{1}{2} (z^{(k+1)^2} - z^{(k)^2}) \beta_{x,xxx}] + \sum_{k=1}^i \bar{Q}_{16}^{(k)} [v_{,xx}^0 (z^{(k+1)} - z^{(k)})] \quad (18-2)$$

$$\frac{\partial \tau_{xy}^{(k)}}{\partial x} = \bar{Q}_{16}^{(k)} [u_{,xx}^0 + z^{(k)} \beta_{x,xx}] + \bar{Q}_{66}^{(k)} [v_{,xx}^0] \quad (19-1)$$

$$\int_{free}^z \frac{\partial \tau_{xy}^{(k)}}{\partial x} dz = \sum_{k=1}^i \bar{Q}_{16}^{(k)} [(z^{(k+1)} - z^{(k)}) u_{,xx}^0 + \frac{1}{2} (z^{(k+1)^2} - z^{(k)^2}) \beta_{x,xx}] + \sum_{k=1}^i \bar{Q}_{66}^{(k)} [v_{,xx}^0 (z^{(k+1)} - z^{(k)})] \quad (19-2)$$

Instead of taking numerical derivatives of u^0 , β_x and v^0 to obtain $u_{,xx}^0$, $\beta_{x,xx}$ and $v_{,xx}^0$, their expressions can be obtained from the governing equations of the joints (which provide expressions for $u_{,x}^0$, $\beta_{x,x}$ and $v_{,x}^0$). For example, for the single-lap and bonded doubler joints, we have the following relations²³,

$$\begin{aligned} u_{,xx}^{0i} &= k_{1i} N_{xx,x}^i + k_{2i} N_{xy,x}^i + k_{3i} M_{xx,x}^i \\ \beta_{x,xx}^{0i} &= k_{4i} N_{xx,x}^i + k_{5i} N_{xy,x}^i + k_{6i} M_{xx,x}^i \\ v_{,xx}^{0i} &= k_{7i} N_{xx,x}^i + k_{8i} N_{xy,x}^i + k_{9i} M_{xx,x}^i \end{aligned} \quad (20)$$

where k_{ji} are terms containing the laminate stiffness constants and the superscripts $i=1,2$ denote the adherend 1 and 2 respectively (see Mortensen²³ for details). The expressions for the x-derivatives of the force and moment resultants appearing in Eq.(20) are obtained from the equilibrium equations (6-7) together with the adhesive constitutive relations. These expressions are, in the overlap region,

$$\begin{aligned} N_{xx,x}^1 &= \frac{G_a}{t_a} u_0^1 + \frac{G_a t_1}{2t_a} \beta_x^1 - \frac{G_a}{t_a} u_0^2 + \frac{G_a t_2}{2t_a} \beta_x^2 & N_{xx,x}^2 &= -\frac{G_a}{t_a} u_0^1 - \frac{G_a t_1}{2t_a} \beta_x^1 + \frac{G_a}{t_a} u_0^2 - \frac{G_a t_2}{2t_a} \beta_x^2 \\ N_{xy,x}^1 &= \frac{G_a}{t_a} v_0^1 - \frac{G_a}{t_a} v_0^2 & N_{xy,x}^2 &= -\frac{G_a}{t_a} v_0^1 + \frac{G_a}{t_a} v_0^2 \\ M_{xx,x}^1 &= Q_x^1 + \frac{G_a(t_1+t_a)}{2t_a} u_0^1 + \frac{G_a t_1(t_1+t_a)}{4t_a} \beta_x^1 & M_{xx,x}^2 &= Q_x^2 + \frac{G_a(t_2+t_a)}{2t_a} u_0^1 + \frac{G_a t_1(t_2+t_a)}{4t_a} \beta_x^1 \\ & - \frac{G_a(t_1+t_a)}{2t_a} u_0^2 + \frac{G_a t_2(t_1+t_a)}{4t_a} \beta_x^2 & & - \frac{G_a(t_2+t_a)}{2t_a} u_0^2 + \frac{G_a t_2(t_2+t_a)}{4t_a} \beta_x^2 \\ Q_{x,x}^1 &= \frac{E_a}{t_a} w^1 - \frac{E_a}{t_a} w^2 & Q_{x,x}^2 &= -\frac{E_a}{t_a} w^1 + \frac{E_a}{t_a} w^2 \end{aligned} \quad (21)$$

In the non-overlap region,

$$\begin{aligned} N_{xx,x}^i &= 0 \\ N_{xy,x}^i &= 0 \\ Q_{x,x}^i &= 0 \\ M_{xx,x}^i &= Q_x^i \end{aligned} \quad (i=1,2) \quad (22)$$

Thus, given the solution to the full set of governing differential equations (described in Sections B, C and D), the adherend-level force and moment resultant derivatives represented by Eqs.(21) and (22) can be obtained. Then, these are substituted into Eqs.(18) and (19), allowing the integrals in Eq.(15) to be evaluated as indicated in Eqs. (18-2) and (19-2). Note that $\sigma_{zz}(x,z)$ is still determined via numerical integration of the results for $\tau_{xz}(x,z)$ (see Eq. (15)). The out-of-plane stress field that results from this procedure does not suffer from the oscillations that occur when the integrals in Eq. (15) are simply evaluated numerically.

It should be noted that Eqs. (21) and (22) can take different forms for other joint types. Out-of-plane stresses solved by the above approach are based on the equilibrium equations and the in-plane stresses obtained from CLT. As such, they do not satisfy the free edge boundary conditions, where the shear stresses should equal zero.

III. Numerical Example

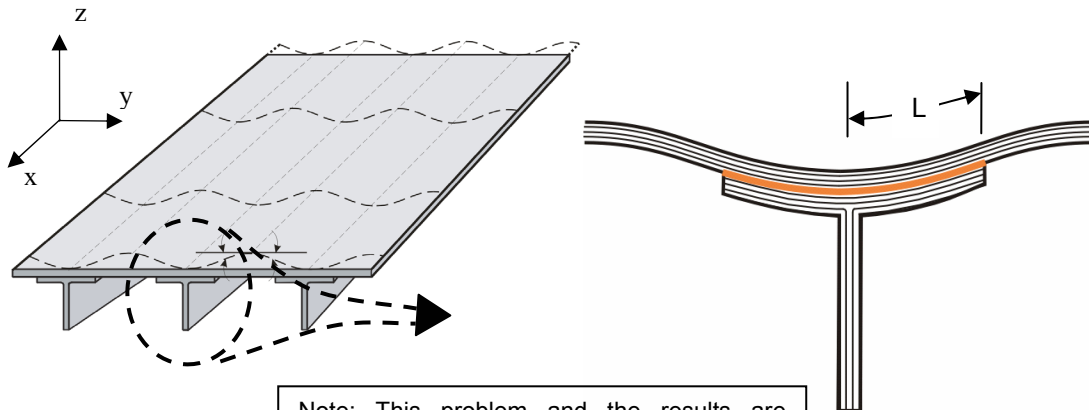
A. Bonded doubler joints with laminated adherends

Joint configuration

The example results presented apply to a bonded doubler joint that is intended to represent a section of a stiffened panel, as shown in Fig. 3. The joint uses laminated adherends with off axis plies subjected to either tensile or bending moment loading. The configuration of the bonded doubler joint is shown schematically in Fig. 3. Adherend 1, which represents the panel facesheet, consists of 18 plies of boron/epoxy prepreg tape with a $[45^\circ/-45^\circ/0^\circ/90^\circ/0^\circ/90^\circ/45^\circ/-45^\circ/0^\circ]_s$ lay-up and a ply thickness of 0.005 in. Adherend 2, representing the stiffener flange, consists of 6 plies of boron/epoxy prepreg tape, with a $[0^\circ/90^\circ/45^\circ/-45^\circ/90^\circ/0^\circ]$ lay-up, and a ply thickness of 0.005 in. The adherends are bonded with an epoxy adhesive film with a thickness of 0.004 in. The mechanical properties of the joint materials are given in Table 1.

Table 1 Material properties used in analyses

	E_1 (Msi)	E_2 (Msi)	E_3 (Msi)	G_{12} (Msi)	G_{31} (Msi)	G_{23} (Msi)	ν_{12}	ν_{13}	ν_{23}
Boron/epoxy	32.4	3.5	3.5	1.23	1.23	1.23	0.23	0.23	0.32
Epoxy	0.445	0.445	0.445	0.165	0.165	0.165	0.348	0.348	0.348
Aluminum	10.0	10.0	10.0	3.84	3.84	3.84	0.30	0.30	0.30



Note: This problem and the results are presented in the *panel* coordinate system above, which is different from that in Fig. 1.

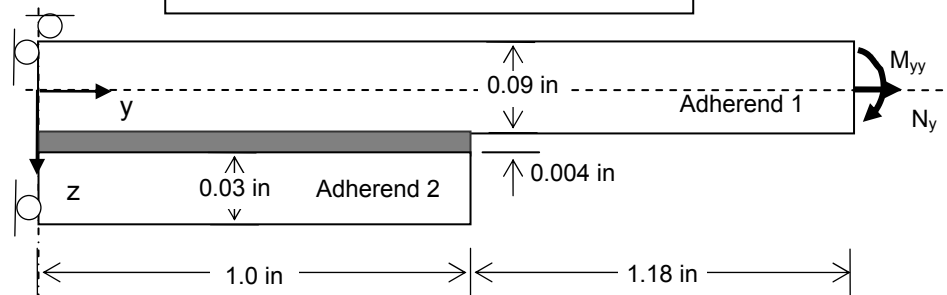


Fig. 3 Configuration of a bonded doubler joint for analysis (not to scale).

Table 2 Geometry, materials and B.C. of stiffened plate

Lay-ups	Loading and Boundary Conditions:
Adherend 1: Boron/epoxy [45°/-45°/0°/90°/0°/90°/45°/-45°/0°] _s , 18 plies Adherend 2: Boron/epoxy [0°/90°/45°/-45°/90°/0°], 6 plies Adhesive: epoxy	Left Face (symmetry): $u_0 = w = \beta_y = v_0 = 0$ Right Face: Case 1: $N_x = 5.71 \text{ lb/in (1 N/mm)}$, $Q_y = N_{yx} = M_{yy} = 0$; Case 2: $M_x = 0.2248 \text{ lb-in/in (1 N-mm/mm)}$, $Q_y = N_{yx} = N_y = 0$; Note: u_0, v_0, w are the displacements of middle plane; β_y is the slope of middle plane with respect to y-axis

Boundary conditions

To correctly model this problem (which is intended to simulate the in-service conditions of an airframe panel, Fig. 3), special attention must be paid to the boundary conditions. In the real situation, the bonded doubler is a part of a stiffened panel such that it is constrained in the longitudinal stiffener (x) direction. HyperSizer models this boundary condition by either constraining the rotation and translation in the axial direction (cylindrical bending), or allowing only constant straining along this direction (generalized cylindrical bending), Fig. 4. The curvature along the longitudinal direction is small compared to that in the transverse direction. Thus, at the left side of the joint shown in Fig. 3, a symmetry boundary condition is applied, while either unit moment or tension is applied at the right side. Table 2 summarizes the boundary and loading conditions applied for each case investigated by HyperSizer.

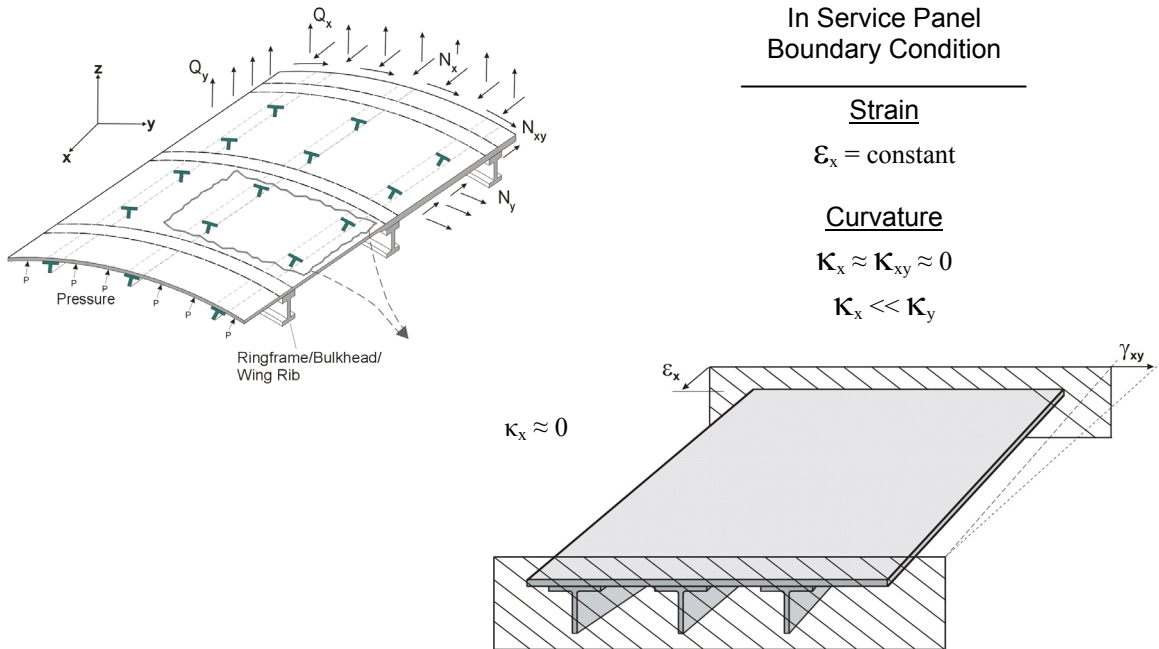


Fig. 4 Boundary conditions on an “in-service panel”.

Consistency Assumptions for FEA Comparisons

The HyperSizer results are compared to results from StressCheck^{12,28}, a p-based finite element analysis package, to verify its through-the-thickness stress calculation. Note that this required explicit modeling of each ply in the StressCheck FEA. The classical lamination theory used by HyperSizer does not account for the effects of transverse shear flexibility. Therefore, to eliminate possible discrepancies this effect could cause between HyperSizer and StressCheck results, the material properties used in the FEA were modified to remove these effects. This means that in the FEA the transverse shear moduli (G_{12} and G_{13}) were set to an arbitrarily high number (1.0×10^8) and the

Poisson ratios that link in-plane to out-of-plane strains (ν_{13} and ν_{23}) were set to zero. All other quantities in the FEA model were set equal to those specified in the problem defined above.

IV. Results and Discussion

A. Rapid calculation of interlaminar and in-plane stresses

One of most important feature of HyperSizer is the capability to calculate local interlaminar and in-plane stresses rapidly. The first example considers the joint subjected to an axial tensile load $N_y = 5.71$ lb/in. Fig. 5 shows the out-of plane shear (red) and peel (black) stresses plotted through the thickness of the joint at several locations progressing toward the free edge of the doubler. The lightest curves start at $y/L = 0.89$ which is about 20 ply

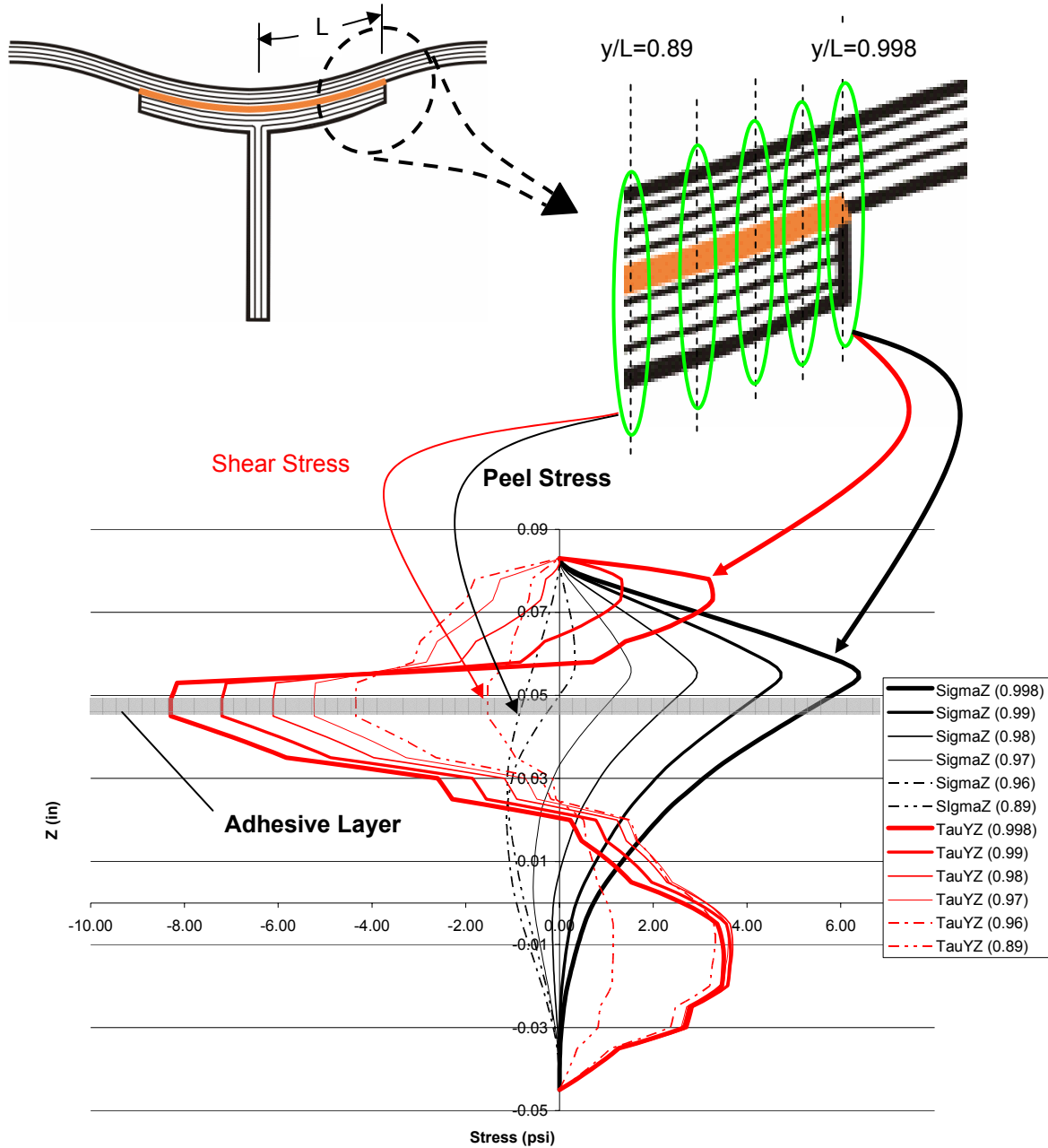


Fig. 5 HyperSizer predictions of the interlaminar stress distributions through the thickness of the joint. Parenthetical values are the y/L location of the plotted stress distribution.

thicknesses away from the free edge and the darkest curve is at $y/L = 0.998$ which is about $\frac{1}{2}$ ply thickness away from the free edge. Notice, especially in the peel stress, that not only do the stress magnitudes vary greatly, but the character of the stress field completely changes close to the free edge. Similar plots are given for the through-the-thickness distribution of the adherend in-plane stresses at the middle point of overlap ($y/L = 0.5$) and at the free edge ($y/L = 1.0$), as shown in Fig. 6. The results show clearly the step-wise distribution of in-plane stresses due to discontinuities of material properties between plies.

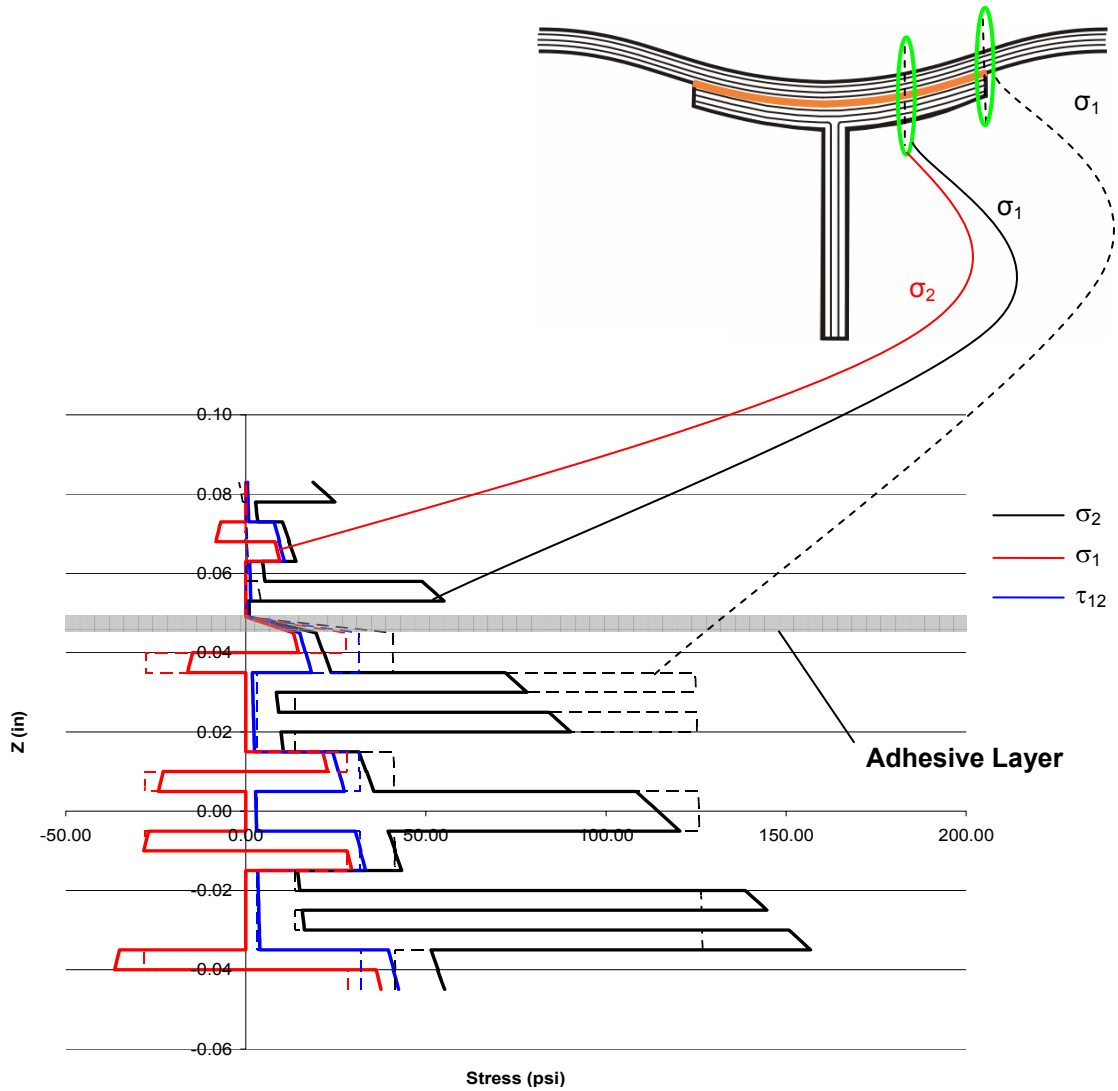


Fig.6 HyperSizer predictions of the in-plane stress distributions through the thickness of the joint.

B. Comparison of HyperSizer results with FEA

Two verification cases were studied for the bonded doubler shown in Fig. 3 and the results are verified with FEA (StressCheck¹²). In the first case, the joint is subjected to a tensile force $N_y = 5.71$ lb/in; the second case is that the joint is subjected to a bending moment $M_{yy} = 0.2246$ lb - in/in.

Figs 7-11 show the results for case 1. Fig. 7 indicates very good agreement between StressCheck and HyperSizer results of the middle-plane deflection of adherends. The ratio of span to thickness of the adherends is greater than 20:1, such that even if transverse shear was considered in the FEA, HyperSizer's CLT would still generate very similar results. Fig. 8 shows the comparison of StressCheck and HyperSizer results for the adhesive shear and peel

stresses along the bondline. The FEA results for comparison are those at the middle of the adhesive layer. Starting at $x/L = 0$, both shear and peel stresses remain almost zero until they reach the region within 20% bondline length away from the free edge, where the peel stress first drops (“trough region”) and then increases dramatically. Shear stresses increase continuously, reaching a maximum at the free edge. The adhesive stresses predicted by HyperSizer are in good agreement with the predictions of the FEA. The shear stresses predicted by the two methods match extremely well, except for the values at the free edge, where the FEA results drops to zero but the HyperSizer solution does not. This free edge behavior is inherent to the spring-type model used for the adhesive layer in the HyperSizer analysis. The peel stresses predicted by the two methods match generally well, but it appears that the HyperSizer’s solution in the “trough” region is more conservative than FEA’s. The maximum point-wise difference between the two methods for the peel stress in the trough region is as high as 50%. Since the transverse shear effect of adherends has been artificially ruled out in FEA, this error is likely caused by the spring-model used in the HyperSizer analysis for the adhesive layer.

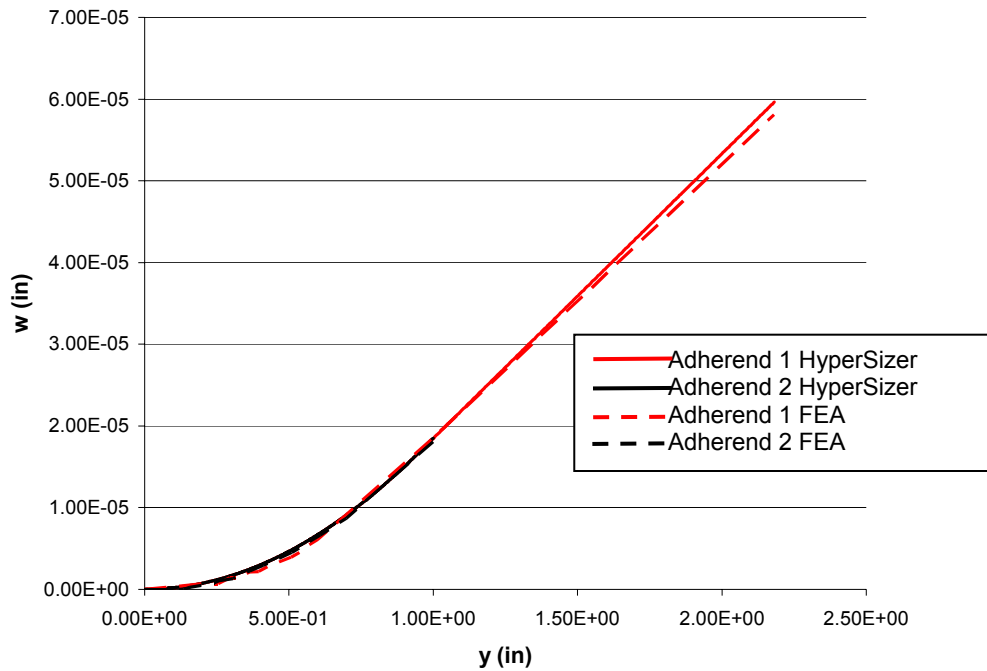


Fig.7 Middle-plane deflection of adherends of the bonded doubler subjected to tension ($N_{yy} = 5.7 \text{ lb/in}$).

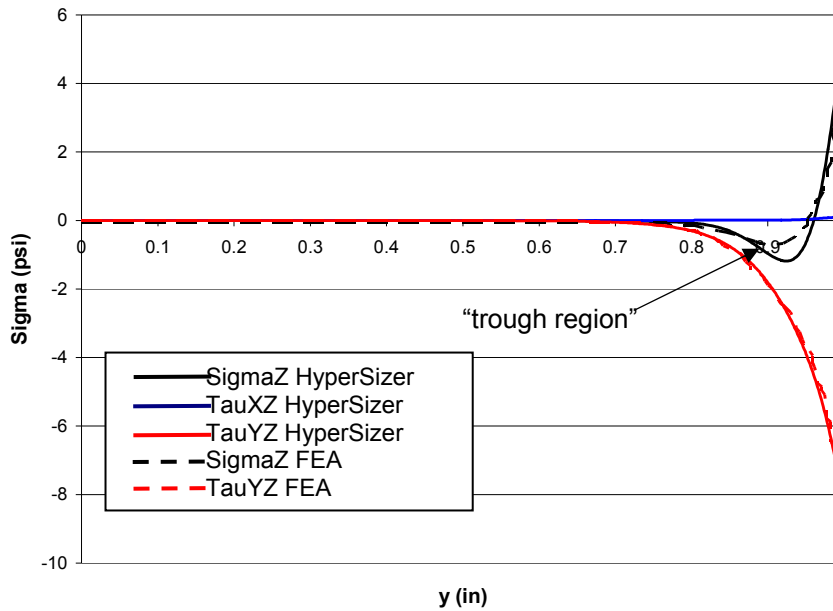


Fig.8 Adhesive shear and peel stresses in the bonded doubler subjected to tension ($N_{yy} = 5.7$ lb/in).

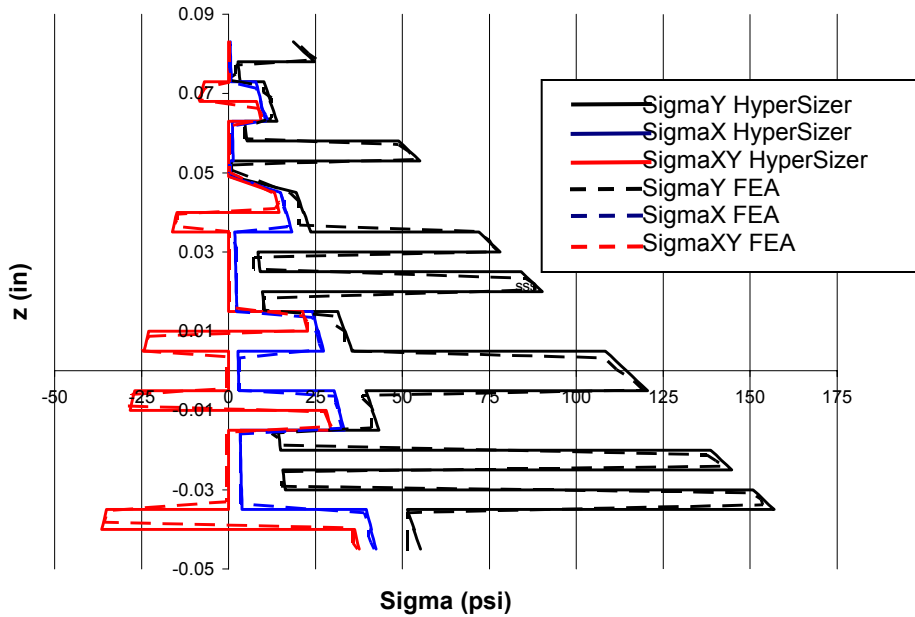


Fig.9 Through-the-thickness distribution of in-plane stresses at $y/L = 0.5$ in the bonded doubler subjected to tension ($N_{yy} = 5.7$ lb/in).

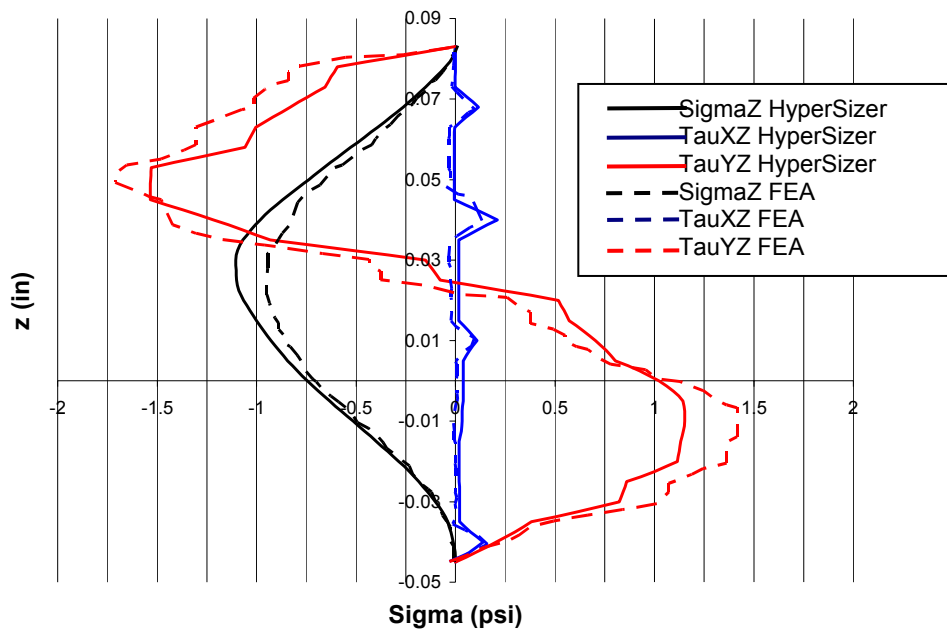


Fig.10 Through-the-thickness distribution of out-of-plane stresses at $y/L = 0.89$ in the bonded doubler subjected to tension ($N_{yy} = 5.7 \text{ lb/in}$).

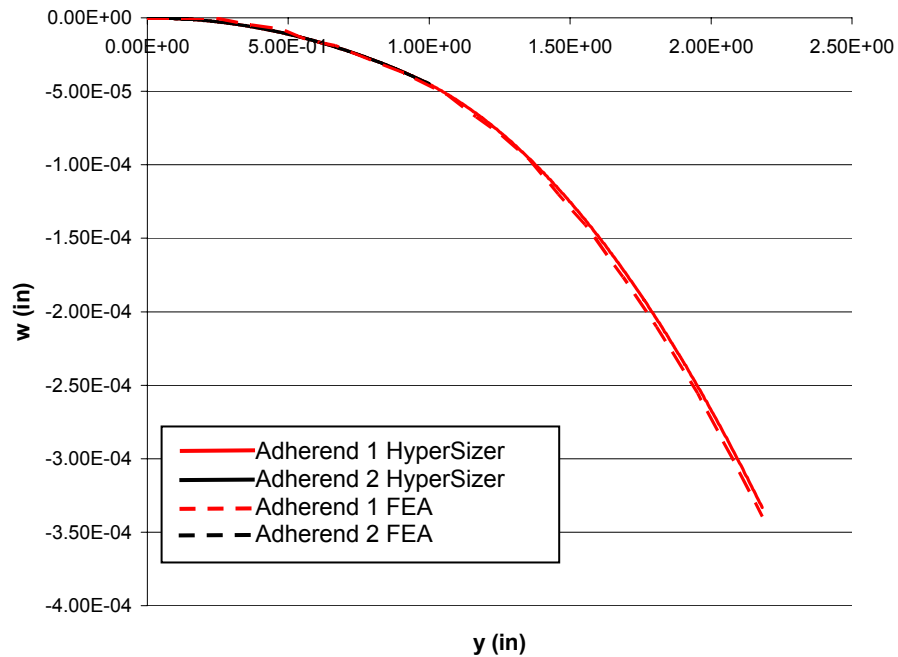


Fig.11 Middle-plane deflection of adherends of the bonded doubler subjected to bending moment ($M_{yy} = 0.2248 \text{ lb.in/in}$).

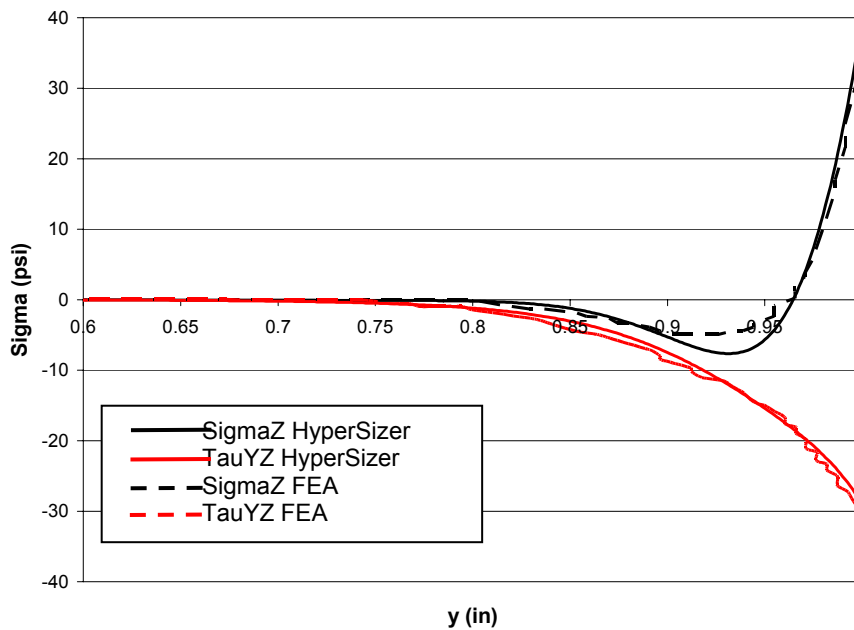


Fig. 12 Adhesive shear and peel stresses in the bonded doubler subjected to bending moment ($M_{yy} = 0.2248 \text{ lb.in/in}$).

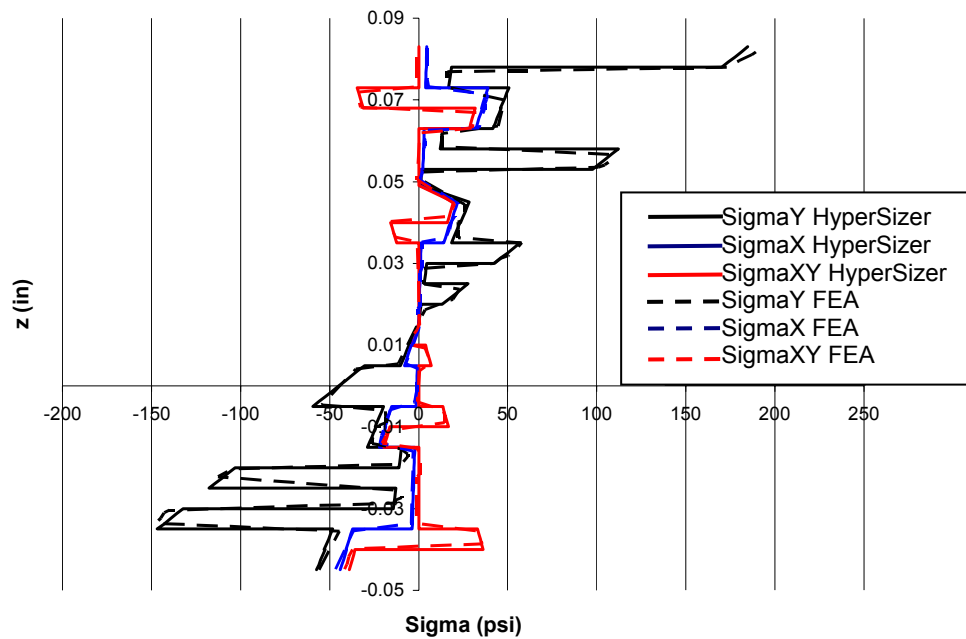


Fig. 13 Through-the-thickness distribution of in-plane stresses at $y/L = 0.50$ in the bonded doubler subjected to bending moment ($M_{yy} = 0.2248 \text{ lb.in/in}$).

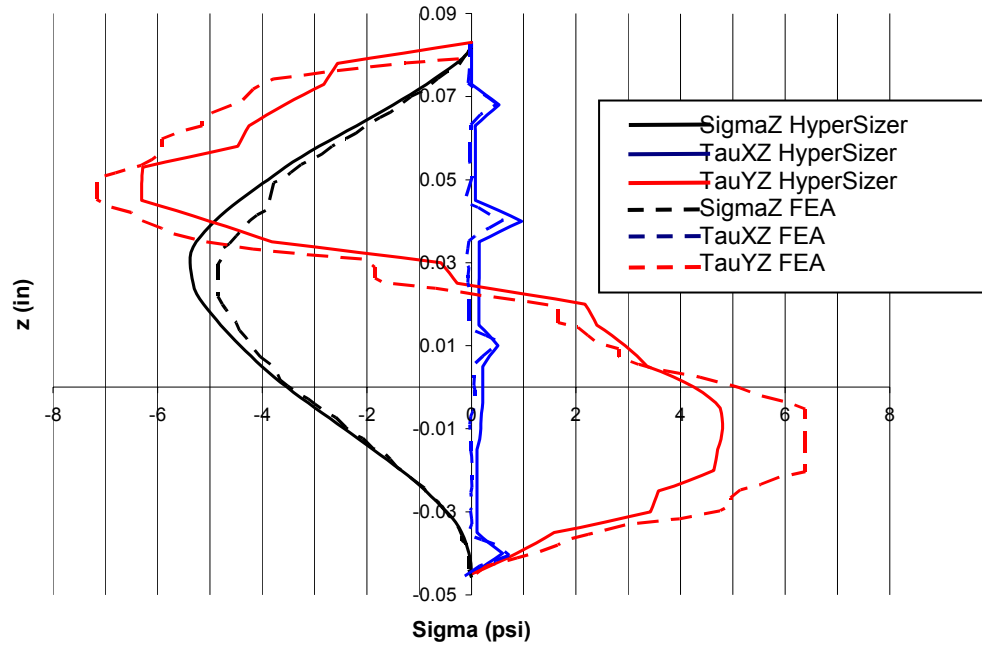


Fig. 14 Through-the-thickness distribution of out-of-plane stresses at $y/L = 0.89$ in the bonded doubler subjected to bending moment ($M_{yy} = 0.2248$ lb.in/in).

Fig.9 shows the comparison of the StressCheck and HyperSizer predictions for the through-the-thickness distribution of in-plane stresses in the adherends. It can be seen that the HyperSizer results match well with the FEA results. Fig.10 shows the comparison of StressCheck and HyperSizer predictions for the through-the-thickness distribution of out-of-plane stresses in the adherends near the free edge, i.e., $y/L = 0.89$. Good agreement is achieved between HyperSizer and FEA and the transverse shear stress shows surprisingly good agreement in particular. At $y/L = 0.89$, the HyperSizer solution for the peel stress does not vary much from FEA's. In general, the largest differences between HyperSizer and the FEA results were in the peel stress calculations. Recalling from the equilibrium equations (15), the longitudinal shear stress τ_{xz} is obtained by integrating of derivative of σ_{xx} , while peel stress σ_{zz} is obtained by integrating the derivative of τ_{xz} . Therefore, any error introduced in the calculation of τ_{xz} will tend to get multiplied in the calculation of the peel stress, σ_{zz} .

Figs.11-14 show the comparison of the same results of HyperSizer and StressCheck for the joint under an applied bending moment $M_{yy} = 0.2248$ lb.in/in. Again, it shows that excellent agreement was obtained for the in-plane stresses, while good agreement was reached for the out-of-plane and adhesive stresses. In both cases, it appears that the spring model used for the adhesive layer affects the results of out-of-plane stresses more than those of in-plane stresses. Recently, Mortensen and Thomsen²⁵ have shown that replacing the linear spring model with a high-order theory model enables better agreement for the adhesive stresses with FEA solutions, especially in the vicinity of free edges. Thus, it is expected the adhesive stresses and adherend interlaminar stresses would be improved through introduction of a more capable adhesive model.

V. Comparison to Other Analytical Methods

The HyperSizer method offers many advantages over traditional analytical methods for bonded joint analysis in that it is capable of handling more general situations, including various joint configurations, both linear and nonlinear adhesive, unsymmetric and unbalanced laminates, more general loading and boundary conditions, and most importantly, computation of local in-plane and interlaminar stresses in composite adherends. The two most widely used analytical methods in the aerospace industry are the Hart-Smith method¹⁵⁻²⁰ and the Erdogan plate method^{21,27}. We briefly described the two methods in Section I.

A. Comparison to Hart-Smith method

The Hart-Smith method has been developed based on Goland and Reissner's¹⁴ theory for a single-lap joint in which the two adherends of the joint were considered as beams and the adhesive layer in the joint was treated as a special kind of "connecting spring" acting between the two beams. Hart-Smith not only extended this approach to a variety of joint types, such as double-lap, scarf and stepped-lap joints, but also modified the approach to incorporate many types of effects such as adhesive plasticity, thermal mismatch and stiffness imbalance. Hart-Smith's efforts resulted in efficient computer codes (one is known as A4EI) for performing parametric studies on a wide array of joint configurations. In addition to the stress analysis, Hart-Smith also characterized the failure modes of bonded joints and developed a series of engineering design rules.

Compared to the Hart-Smith method, HyperSizer method has the following major advantages. First, HyperSizer models the adherends as general classical laminates, which can accommodate multi-axial loads and more general boundary conditions, such as N_x (or u_0), Q_x (or w), M_{xx} (or β_x), and N_{xy} (or v_0), as well as the generation of the reaction forces and moments M_{yy} , M_{xy} , N_y and Q_y . In contrast, Hart-Smith models the adherends as 1-D beams, which can only accommodate N_x (or u_0), Q_x (or w), and M_{xx} . Secondly, HyperSizer can determine the adhesive stresses in terms of the longitudinal shear stress, transverse shear stress and transverse normal (peel) stress. However, Hart-Smith's solution focused on the longitudinal shear stress, giving either the elastic or elastic-perfectly plastic solutions, while neglecting the adhesive peel stress. Hart-Smith believed that the adhesive peel stress could be reduced by appropriate design of the joint and thus should not be an issue. Even though Hart-Smith did not include the peel stress calculation in the joint analysis computer program A4EI, he gave a simplified method for calculating adhesive peel stress in his NASA report for double-lap joints¹⁵. This simplified method assumes that the adhesive shear stress is constant in the presence of peel stress, so that the peel stress solution is totally uncoupled from the shear stress. This assumption is unrealistic and could lead to large errors in the solution for the adhesive peel stress. Thirdly, the shear/tension spring model used by HyperSizer for the adhesive layer is more capable than Hart-Smith's adhesive model in that it can be extended to high-order theory and inclusion of spew fillet effect²³. Fourthly, Hart-Smith method has convergence and precision problem, especially for stepped lap joints. The convergence difficulties are problem dependent, being more severe for brittle (high modulus) adhesives. The underlying difficulty is one of numerical accuracy loss in the presence of extremely high adhesive shear stress gradients at both ends of each of the outer steps. In contrast, HyperSizer solutions have very good convergence and accuracy due to the multi-segment integration method²³ used to solve the differential equations. This numerical method generates very stable solutions for stepped or scarfed joints with either linear or nonlinear adhesives (not just restricted to elastic-perfectly plastic materials). Finally, HyperSizer can solve for both in-plane and out-of-plane stresses in the adherends, while the Hart-Smith method cannot. HyperSizer's 3D stress analysis capabilities enable failure analysis for composite adherends which commonly suffer interlaminar failures. The comparison between the two methods is summarized in Table 3.

Table 3 Comparison of HyperSizer method to Hart-Smith method for bonded joint analysis

	Bonded Joint Analysis by Hart-Smith¹⁵⁻²⁰	Bonded Joint Analysis by HyperSizer
Solver	1-D closed-form solution using beam theory	A closed-form solution based on Mortensen's unified approach and modification.
Joint types	Conventional joints: Single-lap, double-lap, scarfed, and stepped joints.	Conventional joints: Single-lap, double-lap, scarfed, and stepped joints (adherend can be straight or scarfed (ply-drop-off)).
Loads and effects	N_x , Q_x , M_{xx} .	N_x , Q_x , M_{xx} , N_{xy} (N_y , Q_y , M_{yy} and M_{xy} are reaction forces). Also can enter strains and curvatures in any combination with the forces and moments.
	1. Temperature change 2. Adherend imbalance 3. Defects in <i>bond layer</i> , such as porosity, thickness variation are considered, etc.	1. Temperature change 2. Moisture in laminates 3. Electromagnetic effects
Adherends	Linear elastic homogeneous beams, no transverse deformations are accommodated.	Linear elastic classical laminates (could be asymmetric and unbalanced), no transverse deformation is yet accommodated but will be in a

		future release.
	Output: 1. Longitudinal normal stress and strain, as well as displacement (u_0, w). 2. Interlaminar stresses are not available	Output: 1. In-plane stresses, strains, and displacement (u_0, v_0, w). 2. Out-of-plane (interlaminar) stresses are calculated.
Adhesive	1. Shear spring only. 2. Elastic-perfectly plastic material.	1. 2D isotropic linear elastic spring. 2. Several nonlinear material representations. 3. High-order theory (to be developed). 4. Spew fillet effect (to be developed).
	Output: Shear (longitudinal only) stress for most joint types. A simplified method is proposed for solving for the peel stress, which is decoupled from the adhesive shear stress.	Output: Shear (longitudinal & transverse) and peel stresses, which are constants through the thickness by using the spring model, but may vary if using high order theory (HOT).
Convergence of solution	Have stability/convergence problems with stepped-lap joints.	Convergence is more robust.

B. Comparison to Erdogan's method and FEA

The work of Erdogan (and co-workers^{21,27}) on bonded joint analysis resulted in a unified analytical approach for several joint configurations: stepped lap joints, single-lap joints and bonded doublers. The most prominent feature of the Erdogan method is the application of plate theory to joint analysis. However, compared to HyperSizer, the Erdogan method has the following shortcomings: (1) the adherends are orthotropic plates, as such they can only accommodate the loads of N_x (or u_0), Q_x (or w), and M_{xx} ; (2) the Erdogan method does not solve for the out-of-plane stresses of adherends so that it can not be used to predict adherend interlaminar failures. To further explore the differences between the two methods, an example bonded doubler studied by Delale et al.²¹ is analyzed with HyperSizer and compared to the original Erdogan results.

The problem definition and coordinate system for the joint geometry is shown in Figure 15. The plate material is aluminum, while the flange material is a unidirectional orthotropic Boron/Epoxy composite. The two adherends are bonded using epoxy adhesive, with thickness of 0.004 in. The material properties are the same as those listed in Table 1. Symmetric boundary conditions are applied at the middle cross-section (i.e., $x = 0$) such that only one-half of the geometry shown in Fig. 15 is analyzed, and a tension or moment load is applied at the right edge of plate.

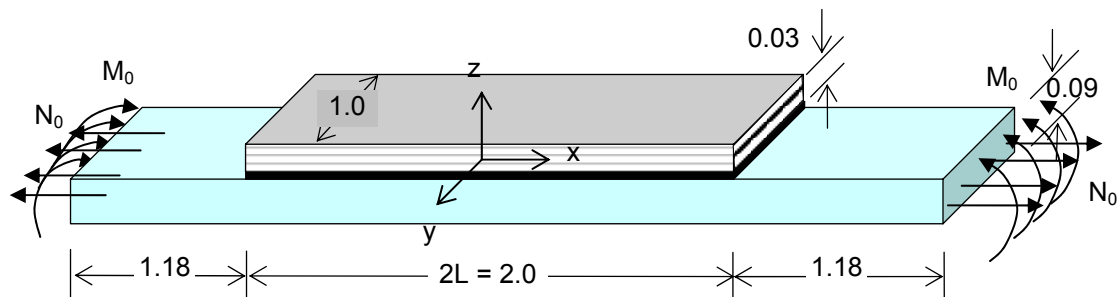


Fig. 15 Stiffened plate (bonded doubler) geometry analyzed by Delale et al²¹. All dimensions are in.

Figs. 16 through 21 show the normalized adhesive longitudinal shear and peel stresses for six different cases of joint tension and moment, and for Alum-Alum adherends and for Alum-B/Ep (Boron/Epoxy) adherends. The last two cases are for the more appropriate in-service panel boundary conditions. Figs. 22 through 26 repeat case 1 of

tension loading for Alum-Alum adherends, but provides more detail data including the effects of linear and non-linear adhesive material properties.

The shear and peel stresses from HyperSizer and Erdogan methods generally match very well with 3D finite element results, except for the peak values near the free edge. It shows that the Erdogan solution exhibits a larger difference for the peak stress at the free edge compared to the FEA result, while HyperSizer has the larger difference for the peel stress in the “trough region”. HyperSizer’s discrepancies in the trough region were described in the example in section III, and are believed to be due to the limitations of the linear spring model. In the present example, the transverse shear stiffness effects of the adherends are not expected to play a large role, due to the large span to thickness ratio of the adherends. Thus, the adhesive model may play an important role in causing the discrepancy in the HyperSizer peel stress in the trough region. It should be noted that the Erdogan method employed an “improved spring model” for the adhesive, which accounts for the effect of longitudinal strain of the adhesive in addition to the shear and peel strain. Thus, improvement of the peel stress in the trough region may be attributable to the usage of this improved adhesive model.

Fig 27 shows failure envelopes for a typical Tee shaped composite stiffened panel. All of the composite laminate failure criteria and bonded joint analyses are included. The ability to generate composite bonded joint failure envelopes are one of the benefits to this rapid analysis capability, as is performing optimization. Fig 28 displays the failure envelope for all relevant stiffened panel analyses and shows how bonded joint strength controls in the tension-tension quadrant, thus the need for this capability during preliminary design and final analysis.

VI. Conclusion

A method for 3D stress analysis of composite bonded joints has been developed. Compared to other analytical methods used for bonded joint analysis, the present method is capable of handling more general situations, including various joint geometries, both linear and nonlinear adhesive, asymmetric and unbalanced laminates, and more general loading and boundary conditions. The new method is based on Mortensen’s unified approach, but it has been considerably extended and modified to enable accommodation of transverse in-plane straining and hygrothermal loads, and, most importantly, to be able to compute the local in-plane and interlaminar stresses throughout the adherends. The present investigation employs HyperSizer to analyze an adhesively bonded composite bonded doubler joint, which represents a section of an aero vehicle stiffened panel. Results have been compared to p-based finite element results (StressCheck), h-based finite element results (ANSYS), and the analytical solution of Erdogan and co-workers²¹⁻²⁷. Good agreement has been achieved between HyperSizer and these other joint analysis methods. The HyperSizer method thus appears to be efficient and generally accurate for analysis of composite bonded joints. It represents a very capable tool for preliminary design, where fast estimates of stress fields, as well as joint strengths and margin of safety are needed.

Acknowledgements

This material is based upon work partially supported by the United States Air Force under Contract.

1. AFRL VA SBIR Phase II contract # F33615-02-C-3216

References

- ¹Collier Research Corp., HyperSizer Structural Sizing Software. Hampton, VA, 2003.
- ²Kairouz, K.C. and Matthews, F.L., “Strength and Failure Modes of Bonded Single Lap Joints Between Cross-Ply Adherends,” *Composites*, Vol.24, No.6, 1993, pp.475-484.
- ³Shenoi, R.A. and Hawkins, G.L., “An Investigation into the Performance of Top-Hat Stiffener to Shell Plating Joints” *Composite Structures*, Vol.30, 1995, pp.109-121.
- ⁴Tsai, M.Y., Morton, J, and Matthews, F.L., “Experimental and Numerical Studies of a Laminated Composite Adhesive Joint” *Journal of Composite Materials*, Vol.29, No.9, 1995, pp.1254-1275.
- ⁵Yamazaki, K. and Tsubosaka, N., “A Stress Analysis Technique for Plate and Shell Built-Up Structures with Junctions and its Application to Minimum-Weight Design of Stiffened Structures,” *Structural Optimization*, Vol.14, 1997, pp.173-183.
- ⁶Tong, L., “An Assessment of Failure Criterion to Predict the Strength of Adhesively Bonded Composite Double Lap Joints,” *J. Reinforced Plastics and Composites*, Vol.6, No.18, 1997, pp.699-713.

⁷Li, G., Lee-Sullivan, P., and Thring, R.W., “Nonlinear Finite Element Analysis of Stress and Strain Distributions Across the Adhesive Thickness in Composite Single-Lap Joints,” *Composite Structures*, Vol.46, 1999, pp. 395-403.

⁸Apalak, Z.G., Apalak, M.K, and Davies, R. “Analysis and Design of Tee Joints with Double Support,” *International Journal of Adhesion and Adhesives*, Vol.16, 1996, pp.187-214.

⁹Krueger, R., Cvitkovich, M.K., O’Brien, T.K., and Minguet, P.J., “Testing and Analysis of Composite Skin/Stringer Debonding Under Multi-Axial Loading,” NASA/TM –1999-209097, NASA Langley Research Center, 1999a

¹⁰Krueger, R., Minguet, P.J., and O’Brien, T.K., “A Method for Calculating Strain Energy Release Rates in Preliminary Design of Composite Skin/Stringer Debonding Under Multi-Axial Loading,” NASA/TM –1999-209365, NASA Langley Research Center, 1999b.

¹¹Bogdanovich, A.E. and Kizhakkethara, I., “Three-Dimensional Finite Element Analysis of Double-Lap Composite Adhesive Bonded Joint Using Submodeling Approach,” *Composite: Part B*, Vol. 30, 1999, pp. 537-551.

¹²ESRD, Inc., www.esrd.com, St. Louis, MO, 2003.

¹³Volkersen, O., “Die Nietkraftverteilung in Ubeanspruchten Nietverbindungen mit Konstanten Loshonquerschnitten” *Luftfahrtforschung*, Vol.15, 1938, pp.41.

¹⁴Goland, M. and Reissner, E., “The Stresses in Cemented Joints,” *Journal of Applied Mechanics* Vol.66, 1944, A17-A27

¹⁵Hart-Smith, L.J., “Adhesive-Bonded Double-Lap Joints,” NASA-CR-112235, NASA Langley Research Center, 1973a.

¹⁶Hart-Smith, L.J., “Adhesive-Bonded Single-Lap Joints,” NASA-CR-112236, NASA Langley Research Center, 1973b.

¹⁷Hart-Smith, L.J., “Adhesive-Bonded Scarf and Stepped-Lap Joints,” NASA-CR-112237, NASA Langley Research Center, 1973c.

¹⁸Hart-Smith, L.J., “Adhesive Bond Stresses and Strains at Discontinuities and Cracks in Bonded Structures,” *Journal of Engineering Materials and Technology*, Vol.100, 1978, pp.15-24.

¹⁹Hart-Smith, L.J., “Differences Between Adhesive Behavior in Test Coupons and Structural Joints,” Douglas Aircraft Company Paper 7066, 1981.

²⁰Hart-Smith, L.J., “Design Methodology for Bonded-Bolted Composite Joints,” Douglas Aircraft Company, USAF Contract Report AFWAL-TR-81-3154, Vol. I & II, 1982.

²¹Delale, F., Erdogan, F., and Aydinoglu, M.N., “Stress in Adhesively Bonded Joints: A Closed-Form Solution,” *J. Composite Materials*, Vol.15, 1981, pp.249-271.

²²Oplinger, D. W., “A layered beam theory for single-lap joints,” Army Materials Technology Laboratory Report MTL TR 91-23.

²³Mortensen, F., “Development of Tools for Engineering Analysis and Design of High-Performance FRP-Composite Structural Elements” Ph.D. Thesis, Institute of Mechanical Engineering, Aalborg University (Denmark), Special Report no. 37, 1998.

²⁴Mortensen, F. and Thomsen, O.T., “Analysis of Adhesive Bonded Joints: A Unified Approach” *Composites Science and Technology*, Vol.62, 2002a, pp.1011-1031.

²⁵Mortensen, F. and Thomsen, O.T., “Coupling Effects in Adhesive Bonded Joints” *Composite Structures*, Vol.56, 2002b, pp.165-174.

²⁶Collier Research Corp., “Consistent Structural Integrity and Efficient Certification with Analysis,” AF SBIR report F33615-02-C-3216, vol.1, vol.2, vol.3, 2004.

²⁷Erdogan, F. and Ratwani, M., “Stress Distribution in Bonded Joints,” *J. Composite Materials*, Vol.5, 1971, pp.378-393.

²⁸ESRD, Inc., Personal Communication, 2003.

Condition 1 – Aluminum-Aluminum Tensile Load

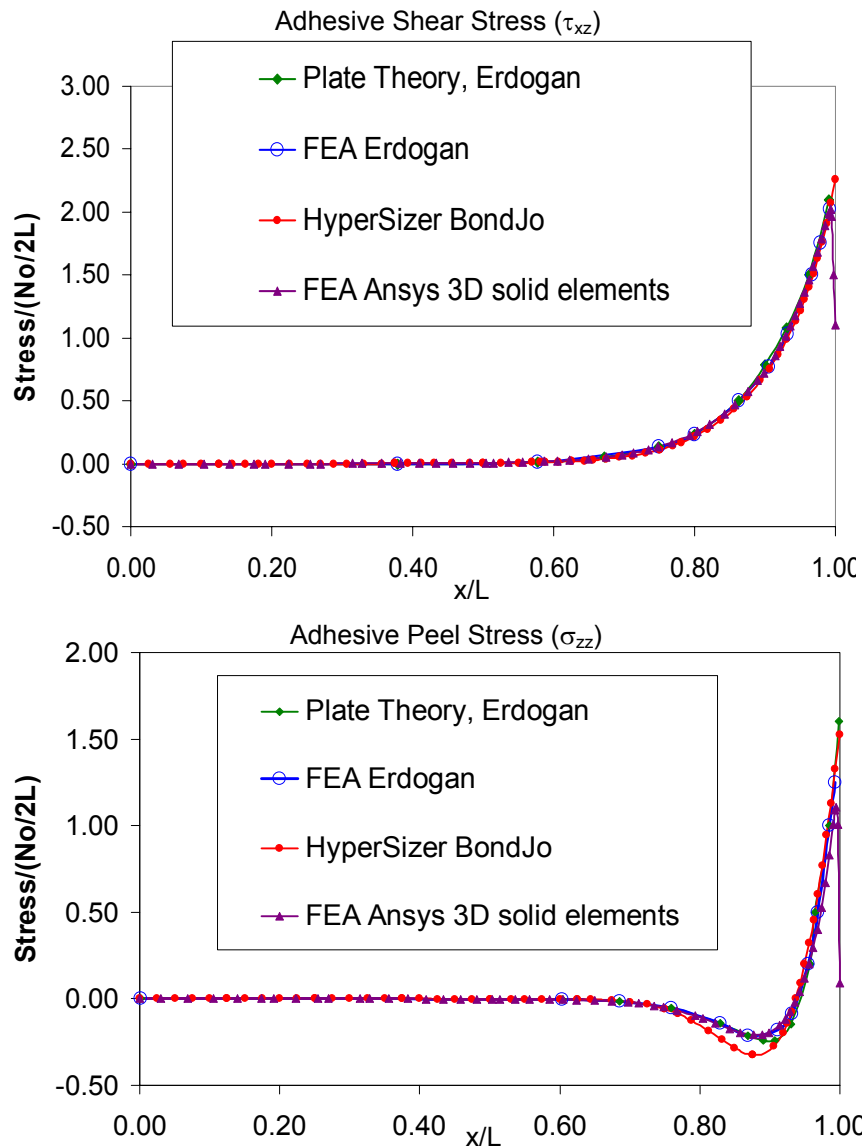
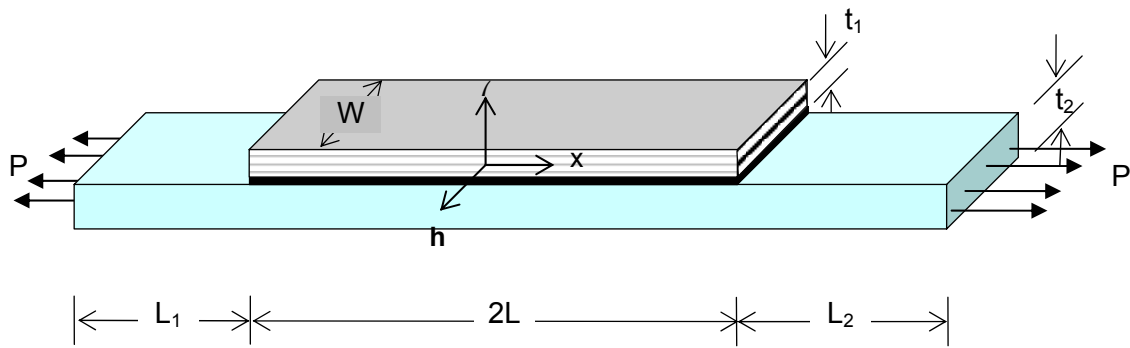


Fig. 16, Adhesive stress comparisons between HyperSizer (BondJo), Ansys solid model FEA and Delale and Erdogan plate theory show good agreement between the codes for adhesive shear but some differences in peel stress in the stress reversal “trough” region. The analytical methods generally and more accurately predict higher peak stresses at the singularity than those of the FEA.

Condition 2 – Aluminum-Aluminum Applied Moment

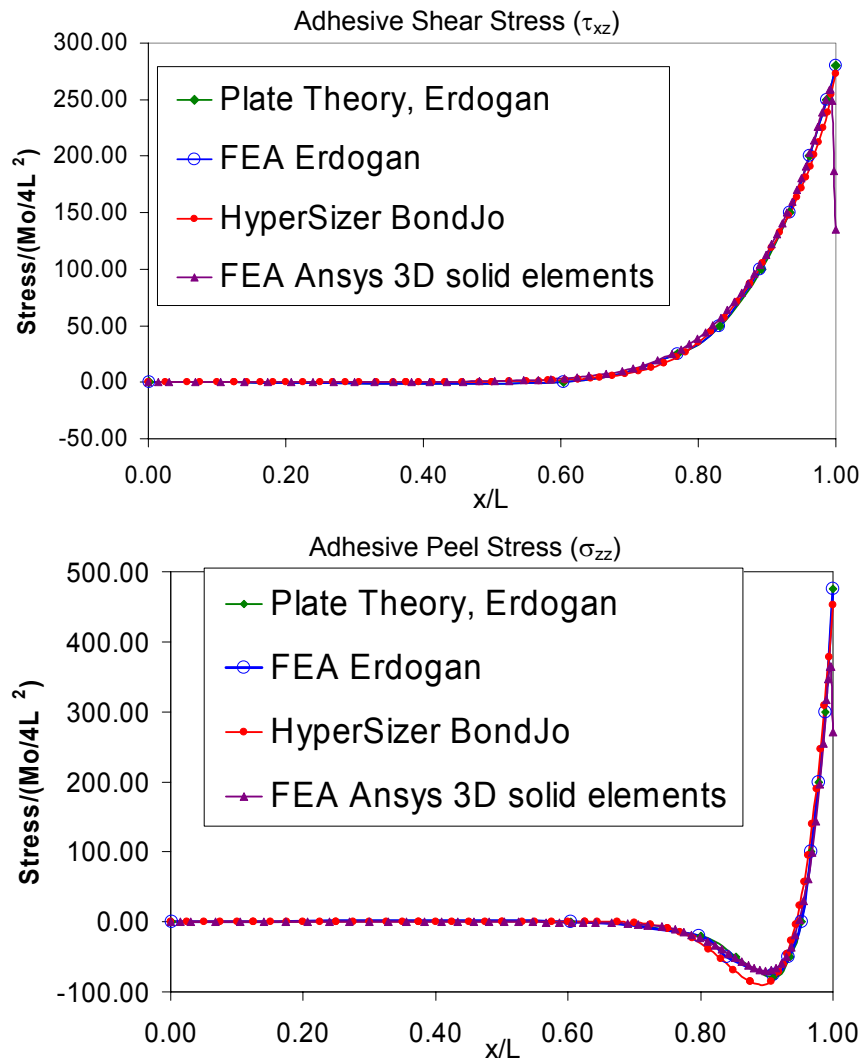
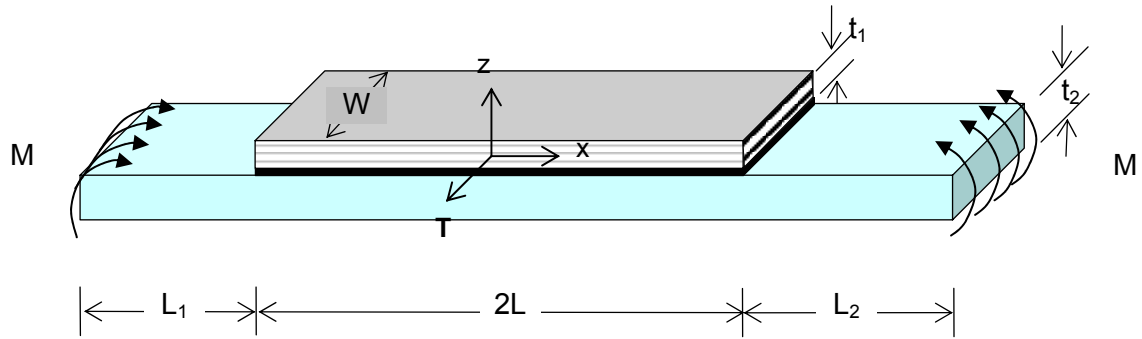


Fig. 17, Adhesive stress comparisons between HyperSizer, Ansys solid model FEA and Delale and Erdogan plate theory show good agreement between the codes.

Condition 3 – Aluminum-BrEp Tensile Load

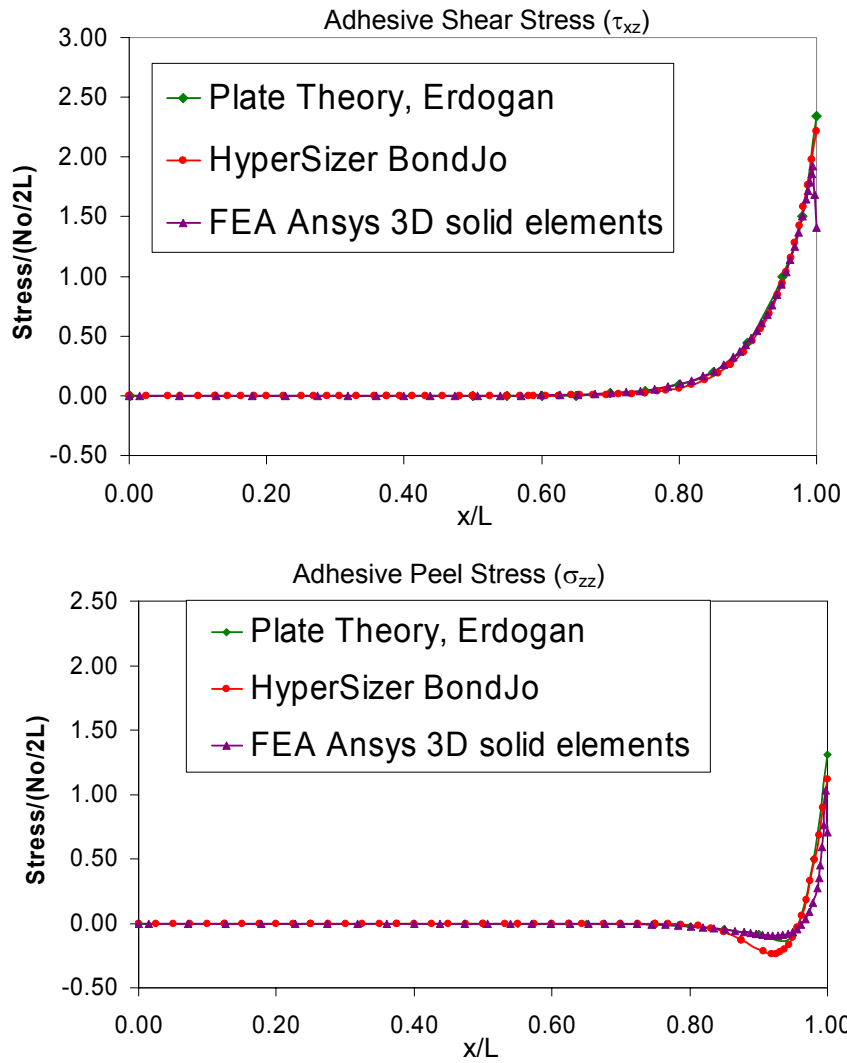
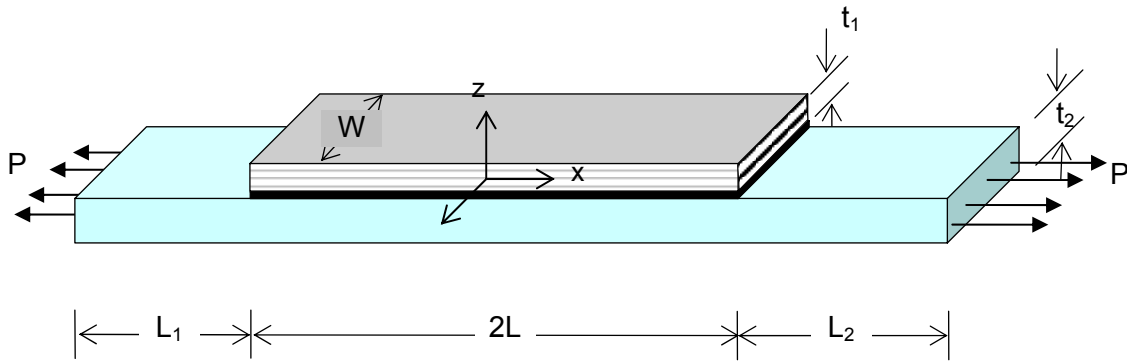


Fig. 18, Adhesive stress comparisons between HyperSizer, Ansys solid model FEA and Delale and Erdogan plate theory show good agreement between the codes.

Condition 4 – Aluminum-BrEp Applied Moment

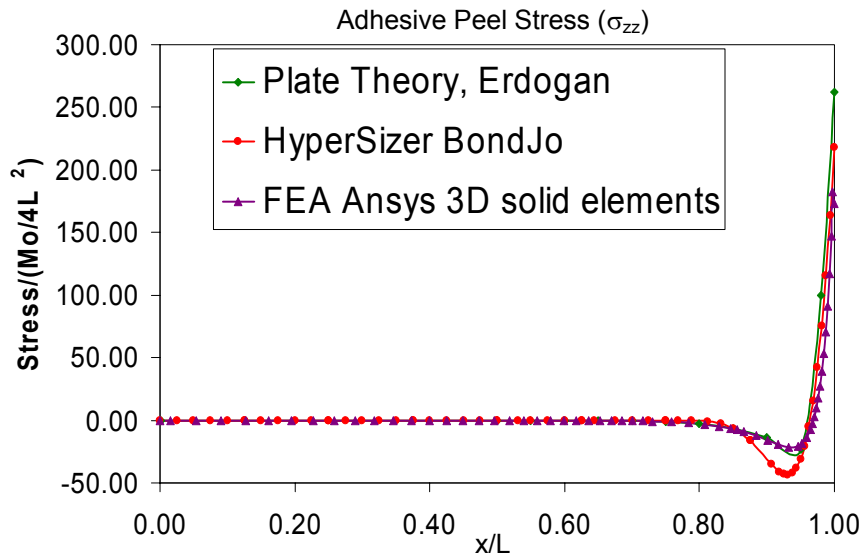
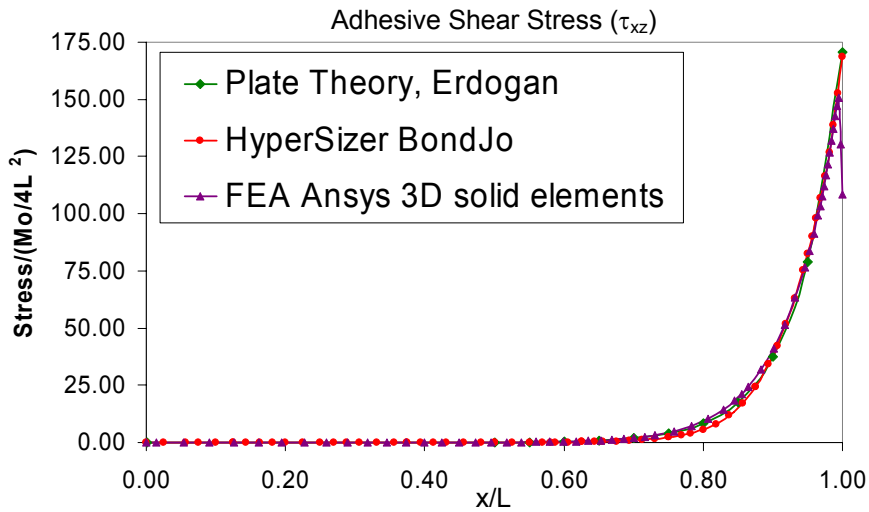
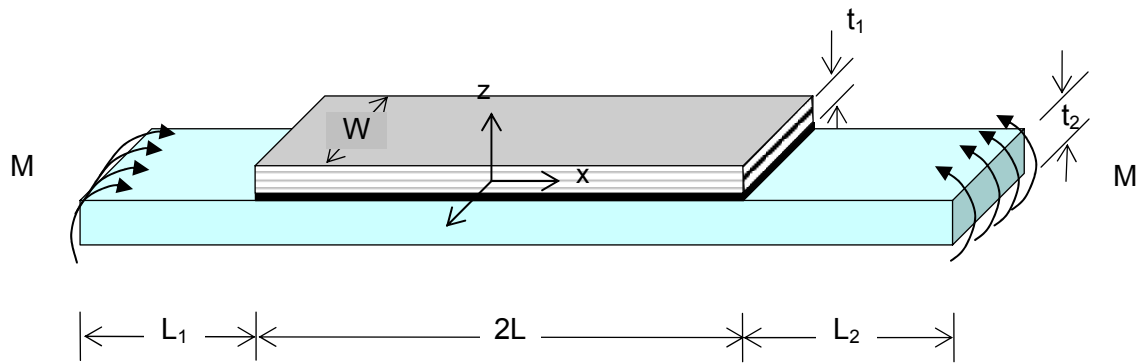


Fig. 19, Adhesive stress comparisons between HyperSizer, Ansys solid model FEA and Delale and Erdogan plate theory show good agreement between the code.

Condition 5 – Aluminum-BrEp In-Service Panel

The following results are presented for the case where the materials and plate dimensions are the same as those presented by Delale and Erdogan, however the boundary conditions have been changed to those that approximate a continuous in-service panel. This boundary condition case, for which HyperSizer was designed, shows very close agreement between HyperSizer and FEA.

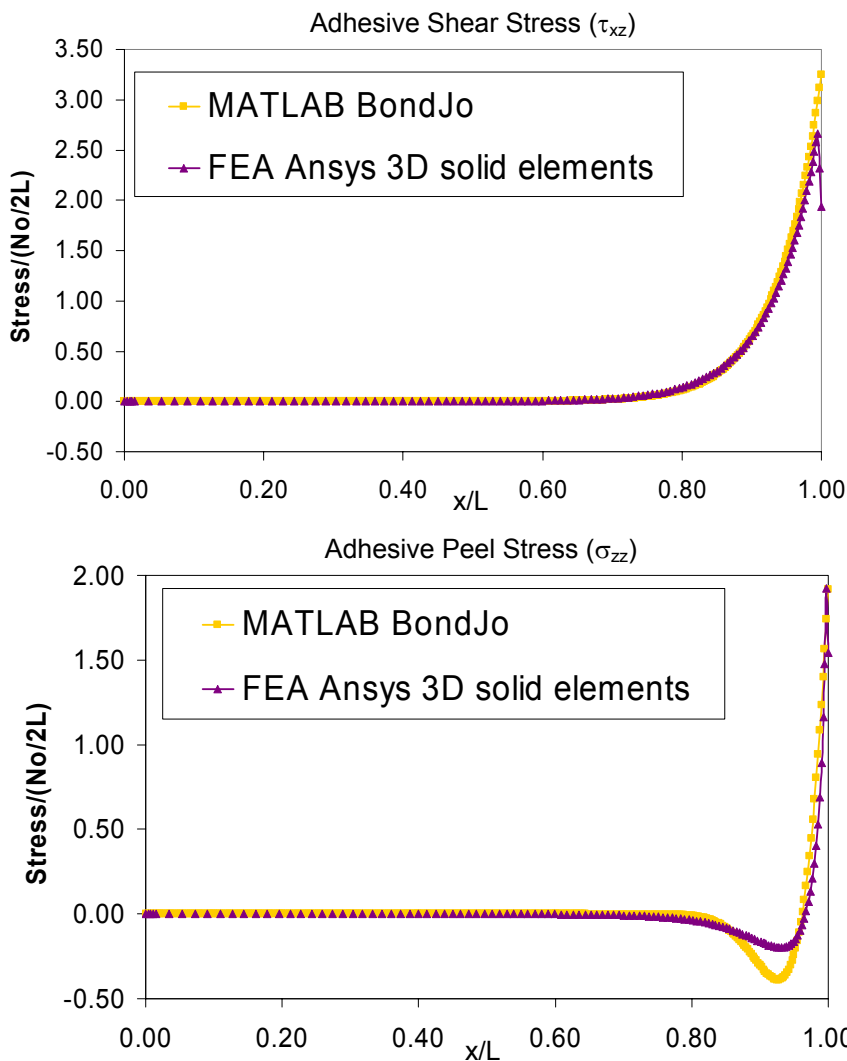
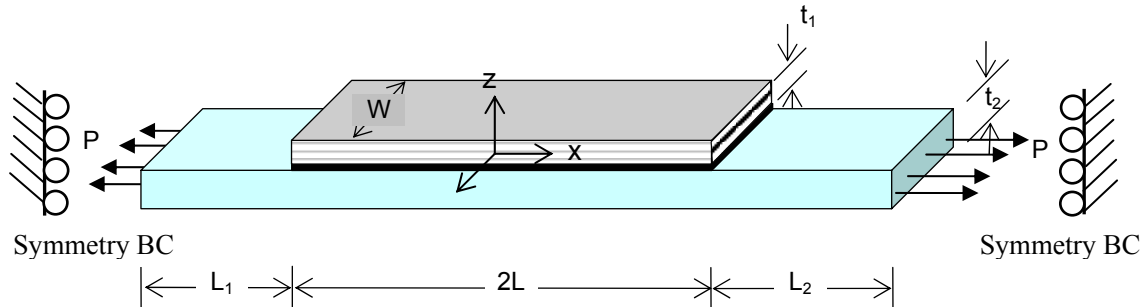


Fig.20, Adhesive stress comparisons between HyperSizer and Ansys solid model FEA show good agreement between the codes.

Condition 6 – Aluminum-Aluminum In-Service Panel

The following results are presented for the case where the materials and plate dimensions are the same as those presented by Delale and Erdogan, however the boundary conditions have been changed to those that approximate a continuous in-service panel. This boundary condition case, for which HyperSizer was designed, shows very close agreement between HyperSizer and FEA.

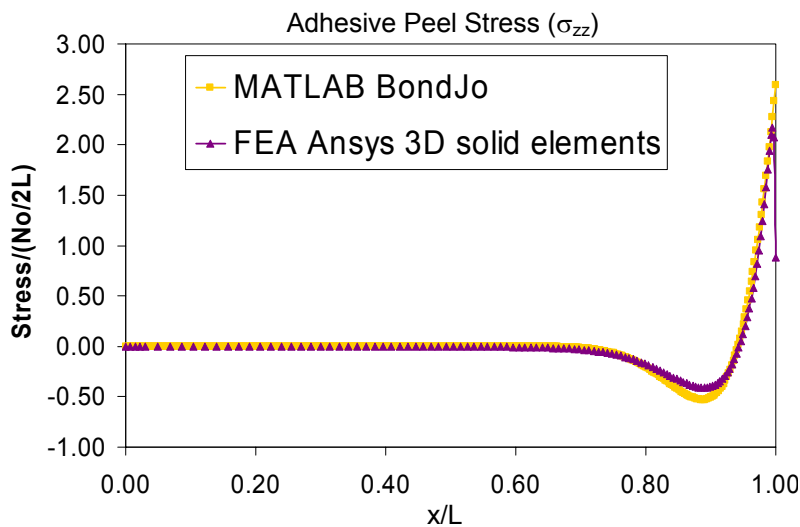
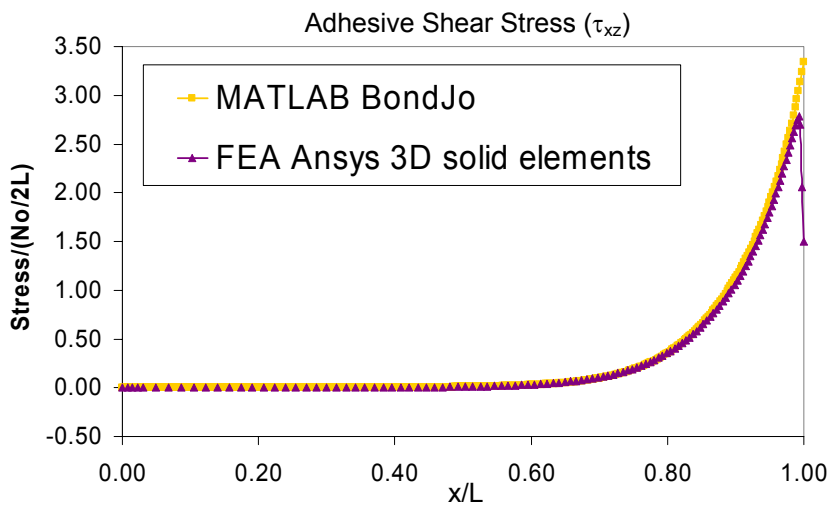
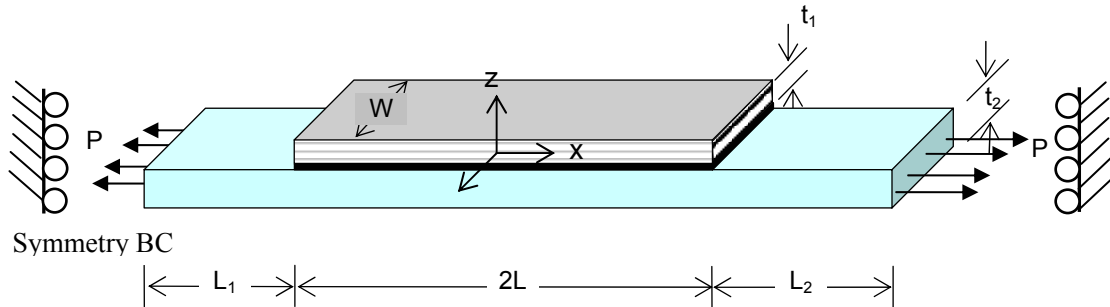


Fig. 21, Adhesive stress comparisons between HyperSizer and Ansys solid model FEA show good agreement between the codes.

Condition 1 – Aluminum-Aluminum Tensile Load [\(Repeated with more results data\)](#)

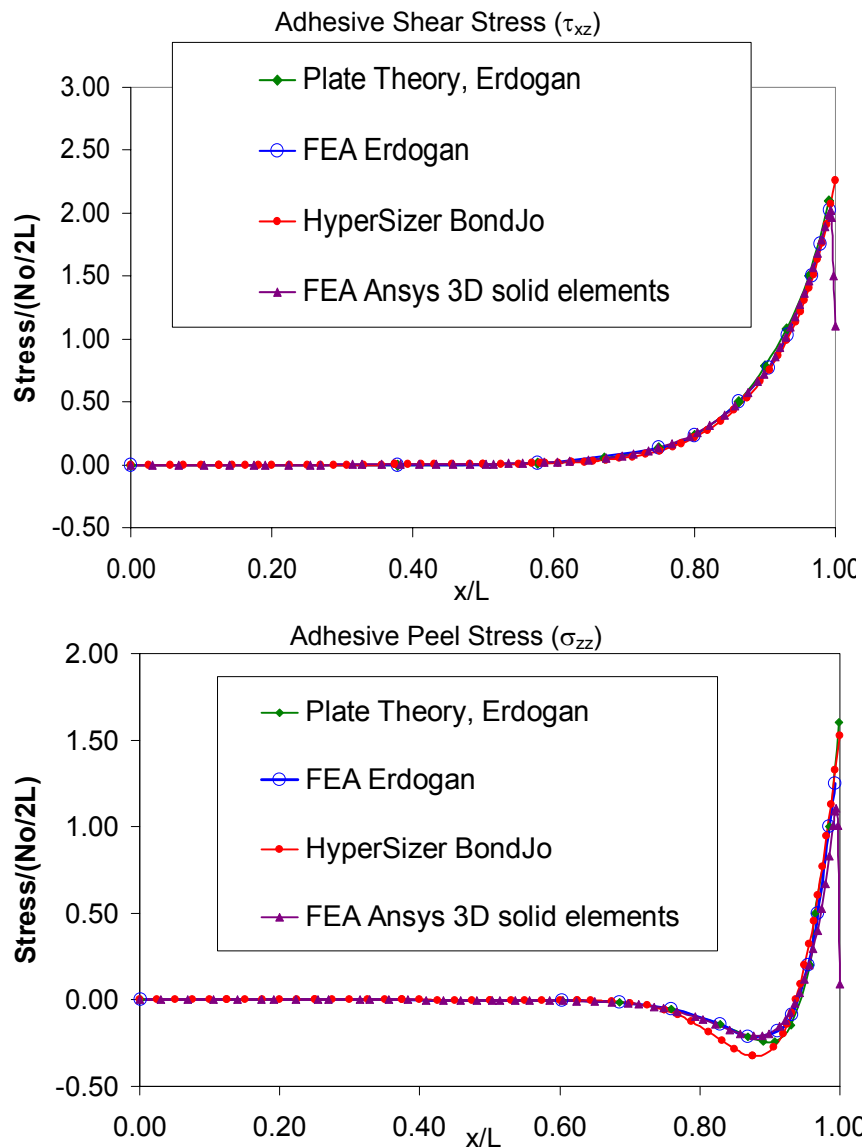
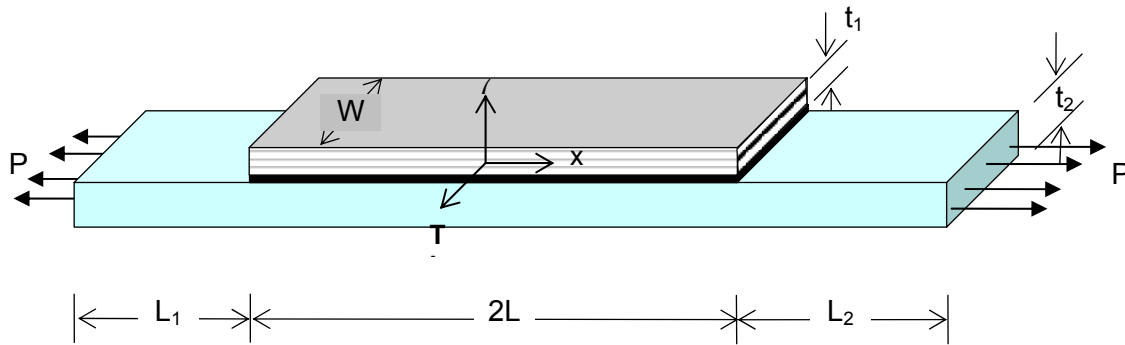


Fig. 22, Adhesive stress comparisons between HyperSizer (BondJo), Ansys solid model FEA and Delale and Erdogan plate theory show good agreement between the codes for adhesive shear but some differences in peel stress in the stress reversal “trough” region. The analytical methods generally and more accurately predict higher peak stresses at the

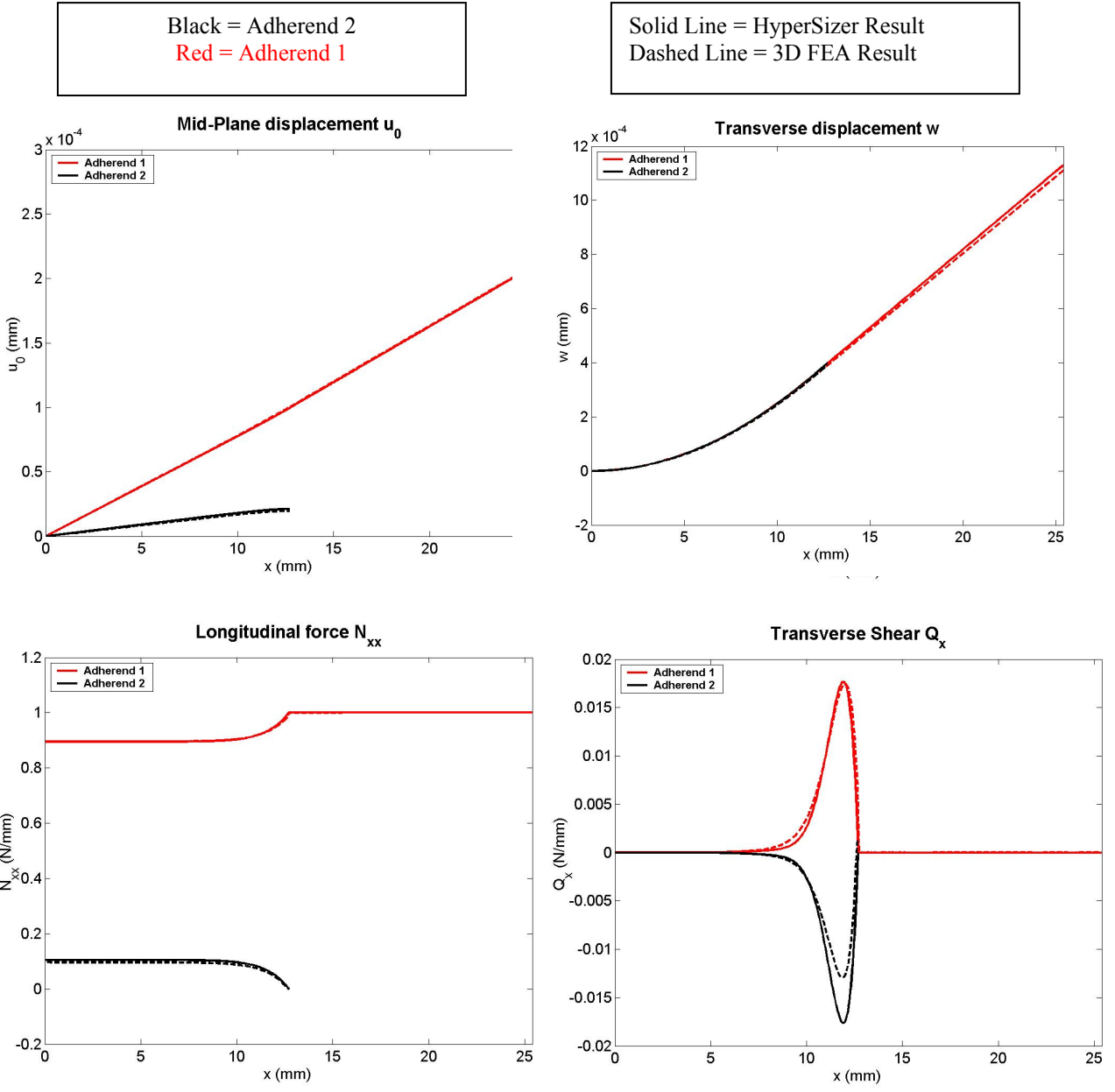


Fig. 23, Displacements and force comparisons.

Black = Peel Stress (σ_z)
 Red = Interlaminar Shear (τ_{xy})
 Blue = Interlaminar Shear (τ_{yz})

Solid Line = HyperSizer Result
 Dashed Line = 3D FEA Result

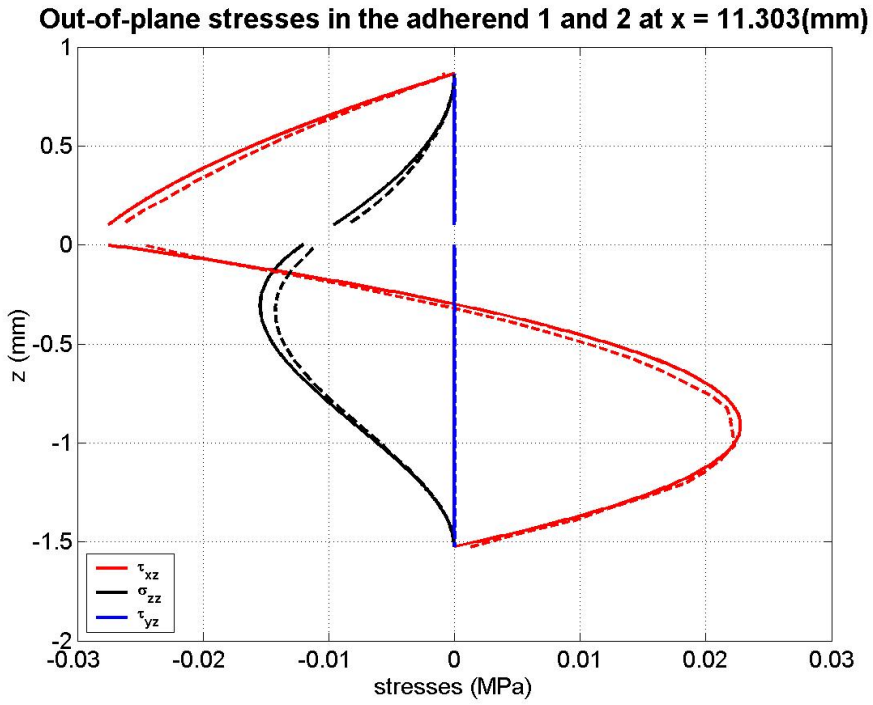


Fig. 24, Out-of-plane stress comparisons.

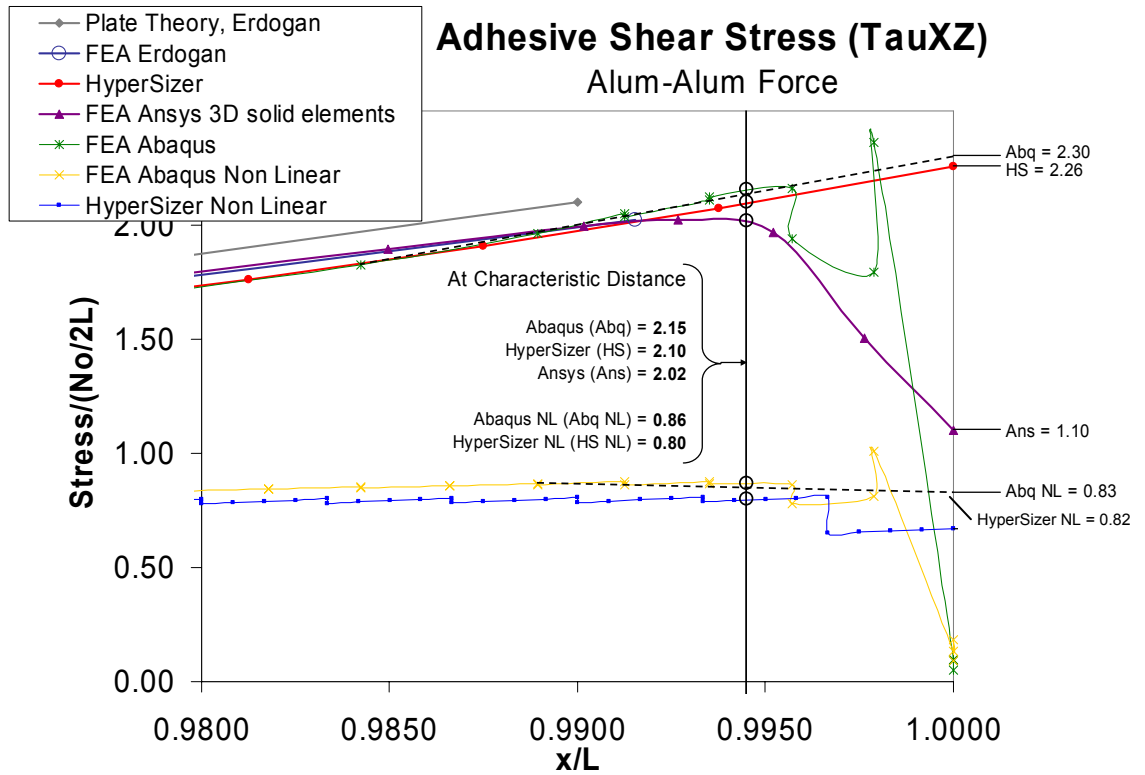
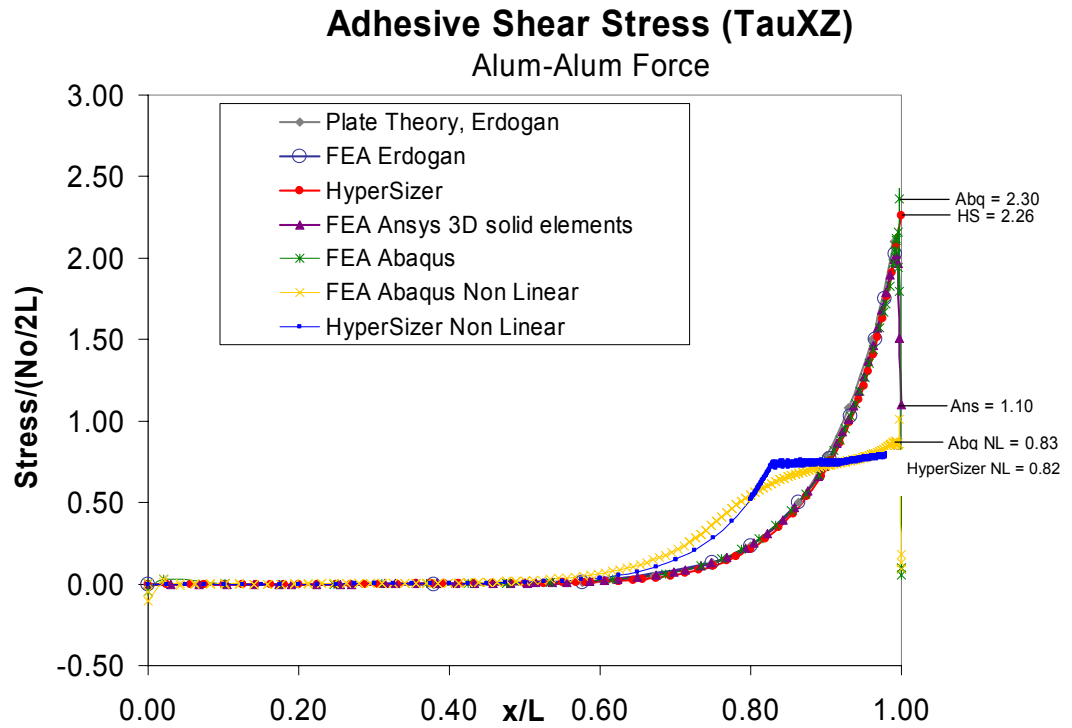
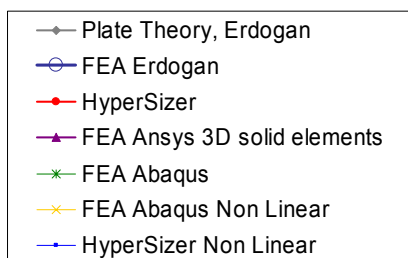
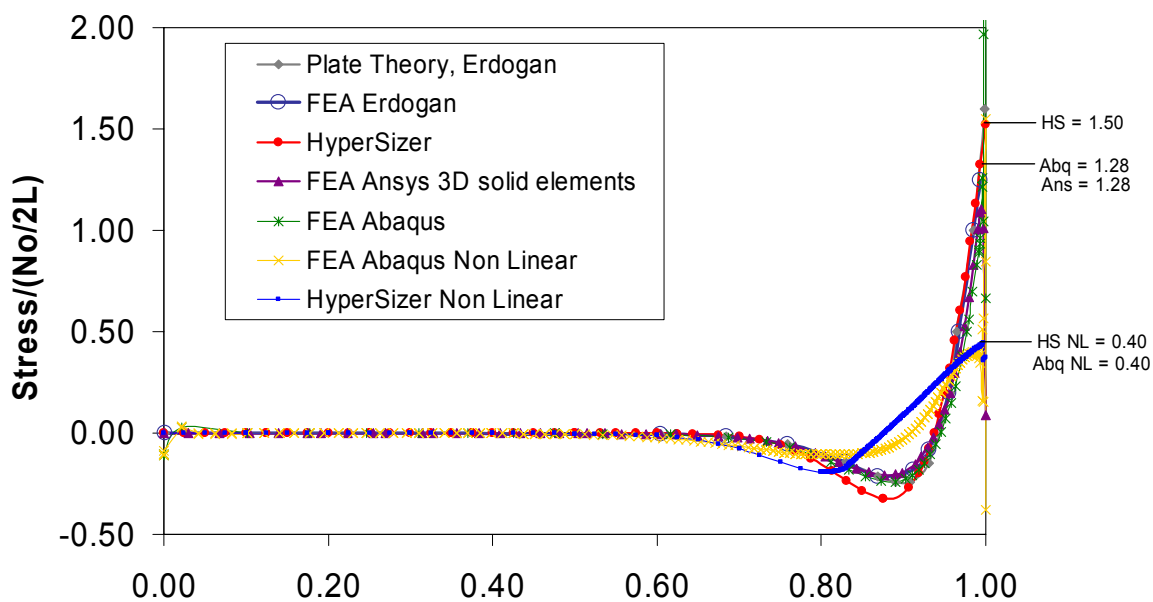


Fig. 25 Detail zoom-in of linear and non-linear comparisons between methods. Note excellent agreement in non-linear results between HyperSizer and Abaqus, even at the reentrant corner (free edge). The results are determined by projecting a straight line from the slope of the curves. HS NL = HyperSizer Non-linear.

Adhesive Peel Stress (σ_Z)

Alum-Alum Force



Adhesive Peel Stress (σ_Z)

Alum-Alum Force

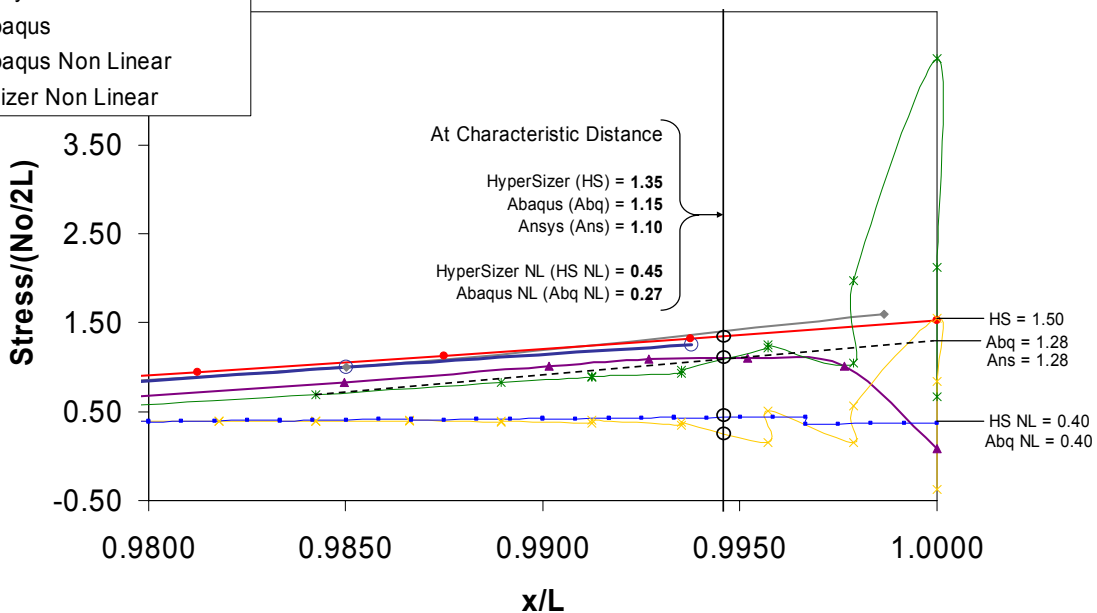
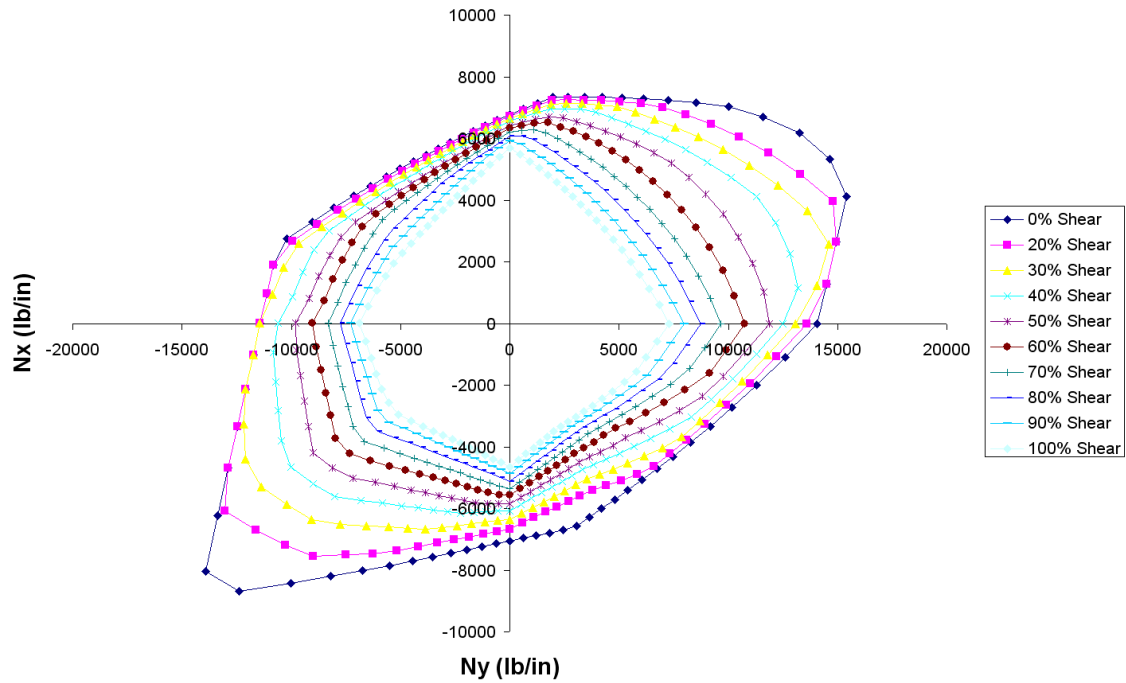


Fig. 26 Detail zoom-in of linear and non-linear comparisons between methods. Note excellent agreement in non-linear results between HyperSizer and Abaqus, even at the reentrant corner (free edge). The results are determined by projecting a straight line from the slope of the curves. HS NL = HyperSizer Non-linear.

Composite Strength Failure Envelopes



Composite Bonded Joint Failure Envelopes

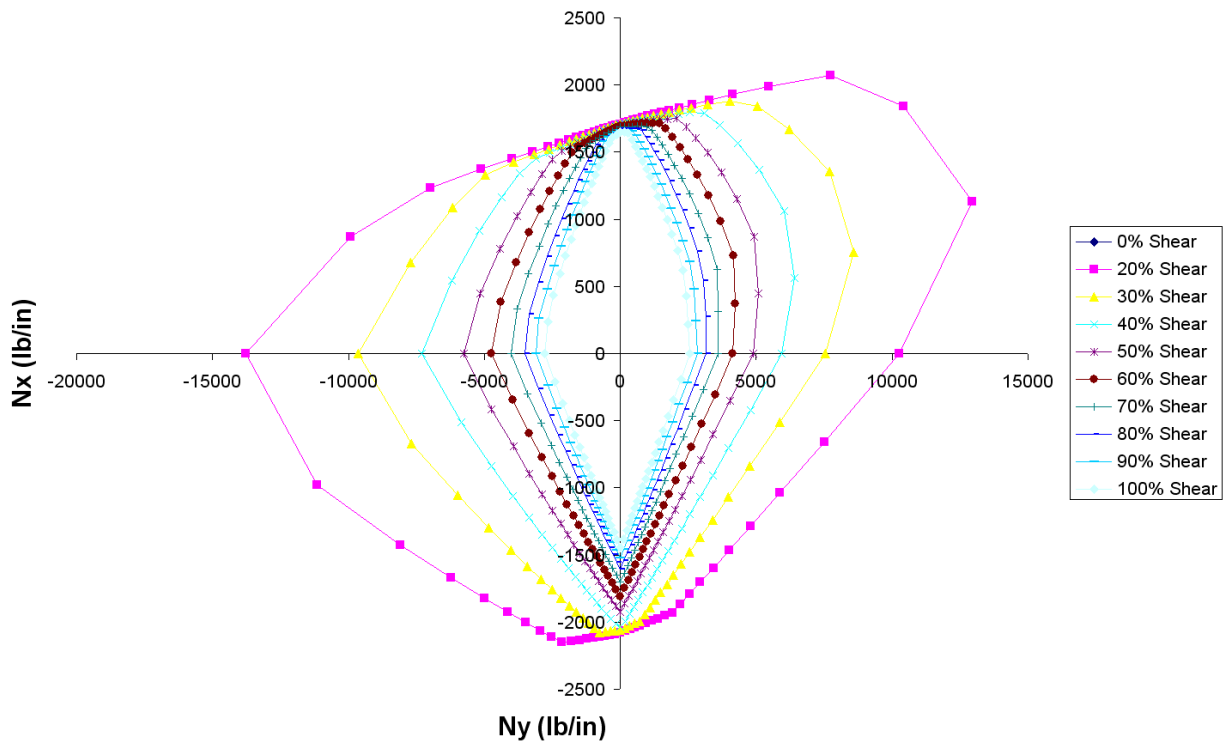


Fig. 27, Top image is the failure envelope for an example composite stiffened panel subjected to a combination of biaxial loadings. Top right quadrant is tension-tension, etc. Using 50% shear as a reference, note how the bottom failure envelope of the composite bonded joint strength has a lower allowable loading, as expected. $N_{x,all}=12,000$ for laminate strength, and $N_{x,all}=5000$ for bond strength.

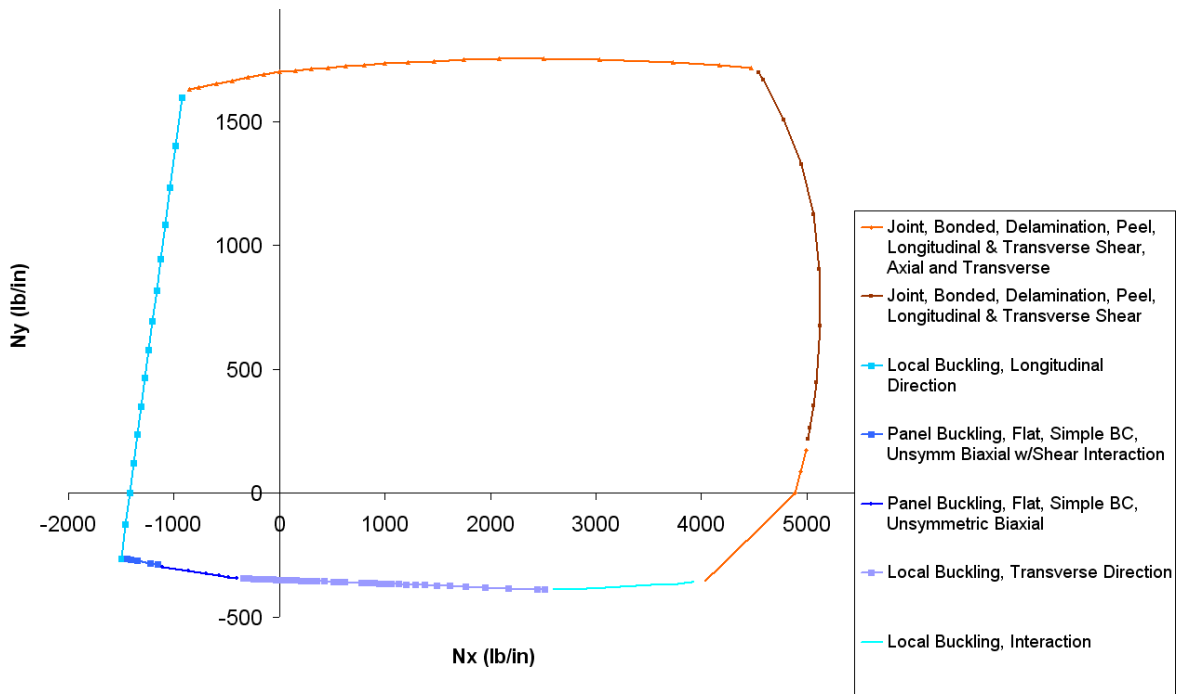
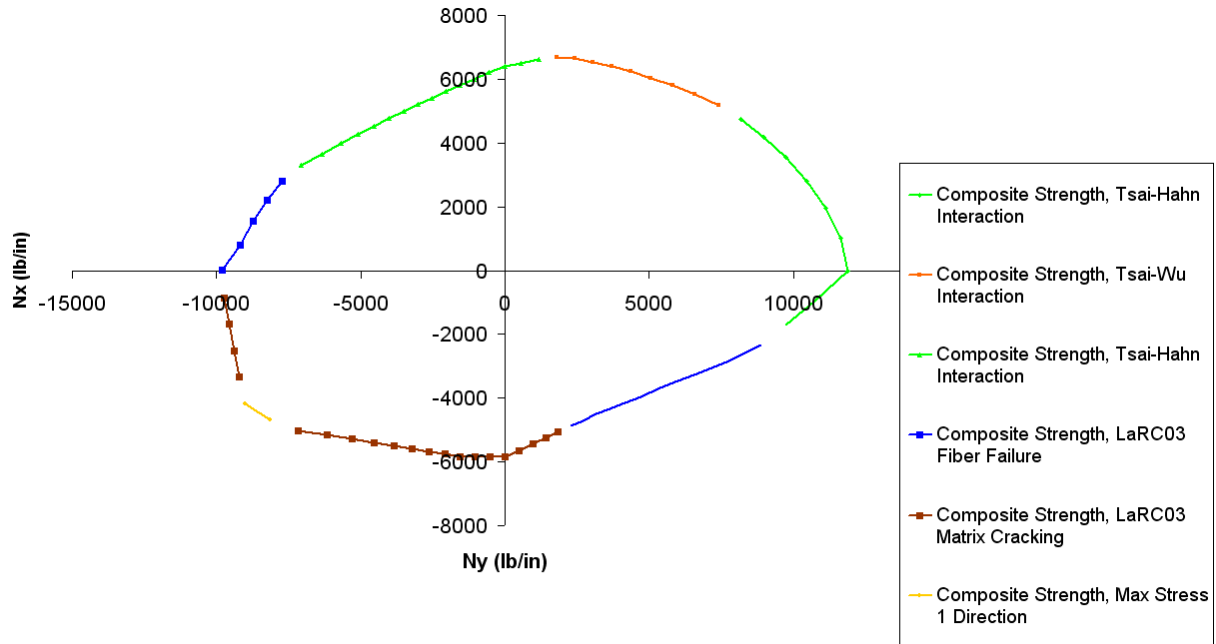


Fig. 28, Using 50% shear as a reference, two failure envelopes are plotted that show controlling failure analysis method. Top image is the failure envelope for different composite failure criteria, and represents the same data that goes into Fig. 27. Note how the bottom failure envelope considers all relevant failure analyses of a stiffened panel, and how the bonded joint strength dominates the tension-tension quadrant, and also portions of the tension-compression quadrants. This proves the need of a rapid joint analysis.